

Mohamed Khider University of Biskra

Faculty of exact sciences Material sciences department

MASTER MEMORY

Sciences de la Matière Physique Physique Energétique et Energies Renouvelables Réf. :

Presented by: **Djellab salsabil**

THE:

Effect of Al, Co, and Al/Co co-doping on the properties of ZnO thin films prepared via Pneumatic Spray Method

Jury:					
Mme	Haif KHaif Ouanassa	MCB	University of Biskra	Presidant	
Mme	Hamani Nadjette	МСВ	University of Biskra	Supervisor	
Mme	Zernadji Raouia	MCB	University of Biskra	Examiner	

Academic Year: 2024/2025

ACKNOWLEDGEMENT

All praise is due to Allah, by whose grace good deeds are accomplished. With His guidance and support, this study has come to completion. I thank Him in the beginning and the end, outwardly and inwardly, as much as has been and as much as will be.

I extend my deepest gratitude and sincere appreciation to my supervisor, **Dr. Hamani**Nadjette, who generously offered her time, expertise, and unwavering support. Her insightful guidance, constructive feedback, and constant encouragement have played a crucial role in overcoming challenges and bringing this work to fruition.

It is a great honor for me that **Dr. Haif Khaif Ouanassa** from Mohamed Khider University of Biskra is the head of the jury for my memory. I am also deeply grateful to **Dr. R. Zernadji** for kindly agreeing to discuss and evaluate my work.

My sincere thanks also go to all the professors, researchers, and students of the Thin Films Laboratory (LPCMA) at Mohamed Khider University of Biskra, whose direct or indirect support, scientific input, and moral encouragement were essential throughout the course of this work.

Finally, I would like to express my profound appreciation to all my esteemed professors in the Department of Material Sciences at the University of Biskra. Their knowledge, guidance, and dedication have been instrumental in shaping my academic journey and inspiring my passion for research and discovery.

DEDICATION

To the one who planted in my heart the love of giving and patience,

To my beloved mother,

All my love and gratitude go to you are the light that illuminated my path and the prayer that accompanied every step of my journey.

To my dear father,

Thank you for your trust, patience, and unwavering presence.

With your strength and support, I have become who I am today.

To my beloved siblings,

You are my strength and pride, my irreplaceable companions on this journey.

Thank you for your constant love and belief in me.

To my dear aunt, who has always been like a second mother,

Your tenderness and heartfelt prayers have meant the world to me. I am forever grateful.

To my beloved cousins,

You were the light in my path and the genuine laughter during times of fatigue.

Your companionship has been an indescribable blessing.

To my dear friends,

You stood by me through every step, offering kindness, support, and warmth.

Thank you for your big hearts and for being a radiant part of my journey.

This work is the fruit of long effort and dedication.

I dedicate it to everyone who truly loved and supported me even with just a word.

From the depths of my heart, I say: without you, I would not be who I am.

With the highest feelings of love and gratitude,

Salsabil Djellab

TABLE OF CONTENTS

ACKNOWLEDGEMENT	
DEDICATION	
CONTENTS	
List of Figures	
List of Tables	
General Introduction	1
CHAPTER I: Overview of TCOs and ZnO	
I.1. Transparent conductive oxide (TCO)	5
I.1.1. Definition of TCO	5
I.1.2 Properties of TCO	6
I.1.2.1 Electrical Properties	6
I.1.2.2 Optical Properties of TCOs:	6
I.1.3. Criteria for Choosing TCO	8
I .2. Zinc Oxide (ZnO)	8
1.2.1. The Choice of ZnO	8
I.2.2. Definition of Zinc Oxide	9
I.2.3. Zinc Oxide Properties	9
I.2.3.1 Structural properties	9
I.2.3.2 Electrical Properties	10
I.2.3.3 Optical Properties	12
I .2.4 Doping of ZnO	12
I.2.5 Co-doped ZnO	14
I.2.5.1 Scope of co-doped ZnO	14
I.2.5.2 CO, Al Co-doped ZnO: ACZO	15
I.2.6 Major applications of zinc oxide	15
References.	19

CHAPTER II: Thin films deposition techniques and characterization methods

	0.6
II.2. Criteria for selection of a deposition technique	
II.3 Choosing the ZnO Deposition Process	
II.3.1. Spray pyrolysis	
II.3.1.1 Definition of spray pyrolysis	
II.3.1.2 Principle	28
II.3.1.3 Model for film deposition by spray pyrolysis	28
II.4. Characterization Methods	30
II.4.1 Thickness Measurements	30
II.4.2. Structural Characterization:	31
II.4.2.1. X-Ray Diffraction	31
II.4.2.2. Measurement of Grain Size, dislocation density and strain	33
II.4.2.3. Determination of Stresses	33
II.4.3. Optical Characterization	35
II.4.3.1.UV-visible spectroscopy	35
II.4.3.2. Optical Band Gap	36
II .4.3.3 Urbach Energy	37
II.4.3.4. Refractive index	38
II.4.4. Morphological Characterization of Thin Films	38
II.4.4.1 .Scanning Electron Microscope (SEM)	38
II.4.5.2. Energy dispersive X-ray spectroscopy (EDS or EDX)	40
II.4.6 Fourier Transform Infrared Spectroscopy (FTIR)	41
II.4.5. Electrical Characterization	42
II.4.5.1 Four-Points Probes Method	42
II.4.5.2 Electrical Resistivity Measurement	43
References	44

CHAPTER III: Experimental result and discussion

III.1 Experimental method50

III.1.1 Pneumatic spray pyrolysis technique
III.1.2 Preparation of substrates and spray solutions
III.1.2.1 Preparation of substrates
III.1.2.2 Preparation of solutions
III.1.2.3 Deposition of thin films
III.2 Results and discussions
III.2.1 Growth rate of the films
III.2.2 Structural study
III.2.2.1 X-ray Diffraction Spectrum (XRD)
III.2.2.2 Crystallite size
III.2.2.3 Dislocation density, strain and stress
III.2.2.4 lattice parameters
III.2.3. Optical properties
III.2.3.1. Transmittance spectra
III.2.3.2 Band gap energy Urbach energy
III.2.4 Electrical properties
Refereces
General Conclusion

List of Figures

Figure I-1: Optical spectra of typical (ZnO) transparent conductor (left side) and schematic electronic str	
of conventional TCO materials (right side) conduction band	7
Figure I-2: Solid zinc oxide in natural form (a) and in the form of a white powder called "white	
zinc"(b)	9
Figure I-3: The ZnO crystal structures, rocksalt, zinc blend, wurtzite	10
Figure I-4: Wurtzite Structure of Zinc Oxide	10
Figure I-5: Structure de bande mesurée pour l'oxyde de zinc en symétrie Wurtzite	11
Figure II-1: Classification of different thin film deposition methods	26
Figure II-2: Spray pyrolysis techniques.	28
FigureII-3: Schematic of aerosol transport by Sears et al	30
FigureII-4: The principle of the diffractometer (XRD)	31
Figure II-5: X-Ray Diffraction	32
Figure II-6: Peak Shift and Strain Type in XRD Pattern	36
Figure II-7: Schematic representation of the UV-Visible spectrophotometer	37
Figure II-8: determination of the gap.	37
FigureII-9 Urbach energy determination.	38
Figure II-10: The interaction of electron beam with specimen and the signal emitted from the sample	39
Figure II-11: A photograph showing three major sections of the SEM: the electron column, the specimen	L
chamber, and the computer control system.	40
FigureII-12: Scheme of X-ray excitations in EDX analysis	41
FigureII-13: infrared spectrometer.	42
FigureII-14: Schematic of a square 4Pprobe configuration.	43
Figure III-1: Spray Pyrolysis Device	50
Figure III-2: Variation of growth rate ZnO / AZO / CZO / ACZO	54

Figure III-3:X ray Diffractogram of thin films	55
Figure III-4: JCPDS NO. 36-1451 folder	56
Figure III-5: XRD patterns of (002) diffraction peak	57
Figure III-6: Values of cristaliune size of thin films	58
Figure III -7: Cristalite size and stain of ZnO /AZO/CZO/ACZO thin films	60
Figure III-8: Variation of Lattice Parameters c and stress in ZnO, AZO, CZO, and ACZO Samples	61
Figure III-9: Lattice parameters a and c of ZnO/AZO/CZO/ACZO	62
Figure III- 10: Transmittance spectra of ZnO/AZO/CZO/ACZO thin films	63
Figure III-11: Variation of average transmittance and thikness of thin films	63
Figure III-12: The plot $(\alpha hv)^2$ versus (hv) for the calculation of the optical band gap energy Eg	64
Figure III-13: Values of the band gap and the Urbach energy of ZnO/AZO/CZO/ACZO films	65
Figure III- 14: Resistivity and Band gap of ZnO/AZO/CZO thin films	66
Figure III -15: Variation of transmittance, conductivity, and quality factor of thin film	67

List of Tables

Table (I-1): Minimum required properties of TCOs.	8
Table (I-2): Optical properties of zinc oxide (ZnO) thin films prepared by different deposition methods	12
Table (I-3): Summary of different doped ZnO thin films as transparent conductors	13
Table (I-4): Summarizes the results of these trials, high lighting variances in the co-doping technique	14
Table (I-5): Al and Co doped and co- doped ZnO.	15
Table:(III-1): Physical and chemical properties of Zinc acetate, Aluminium chloride hexahydrate and Cobalt	chloride
hexahydrate	52
Table (III-2): Experimental conditions.	52
Table (III- 3): Thickness and growth rate of ACZO thin films	53
Table (III-4): crystallite size of thin films	59
Table (III-5): Structural parameters of thin films.	60
Table (III-6): lattice parameters of thin films	61
Table (III-7): Optical properties of thin films.	65
Table (III-8): Electrical properties of thin films.	66

General Introduction

Transparent conducting zinc oxide (ZnO) has recently gained much attention due to the many advantages over other oxide thin films such as In₂O₃, CdSnO₄ or SnO₂. These advantages include non-toxicity, good electrical, optical and piezoelectric behaviours, stability in hydrogen plasma atmosphere and low price [1]. Zinc oxide (ZnO), an n-type semiconductor oxide, has gained much interest for its broad and various applications in optoelectronic, microelectronic and spin transport electronic devices [2].

ZnO is a wide direct band gap energy (3.37 eV), high exciton binding energy (60 meV), high optical transparency in the visible and near-infrared regions, high refractive indices, high electrical properties, high chemical and thermal stability [3].

However, controlling its electrical conductivity remains a major challenge, as ZnO often exhibits unintentional n-type conductivity due to impurities like hydrogen, rather than intrinsic defects as previously believed. Achieving stable and reproducible p-type conductivity is still difficult due to the lack of effective dopants and the presence of compensating centers.

Despite the challenges associated with ZnO's electrical conductivity, recent advancements in material synthesis techniques and a refined understanding of defect chemistry have significantly bolstered its potential in electronic and optoelectronic applications [4,5]. Doping ZnO with various elements is a common approach aimed at enhancing its properties. However, mono doping strategies have largely failed to achieve concurrent improvements in both the physical and optical characteristics of ZnO. This limitation has driven interest toward co-doping methods, which involve the simultaneous incorporation of two different dopants, typically combining group III and group VI elements, to achieve a synergistic enhancement of material properties. Notably, the co-doping system comprising aluminum (Al) and cobalt (Co), despite its promising potential, has not yet been extensively investigated in the scientific literature [6].

ZnO thin films have been prepared using various growth techniques, such as magnetron sputtering deposition [7], sol-gel spin coating [8], pulsed laser [9], and physical vapor deposition [10] Thermal spray technology is considered a simple and cost-effective method for depositing thin films, widely used in applications such as solar cells and glass manufacturing. This technique allows for the preparation of uniform, multilayer films with various components, without the need for high-purity materials, and offers good control over the film's morphology and structure [11].

The main objective of this work is to study the effect of doping ZnO thin films with cobalt (Co) and aluminum (Al) individually, as well as co-doping with both elements simultaneously, on the structural, optical, and electrical properties of the films ZnO, AZO, CZO and ACZO. This research has been divided into three chapters as follows:

✓ CHAPTER I: Overview of TCOs and ZnO

This chapter provides a brief overview of the physical properties of ZnO material and its applications, with a focus on the bibliographic research results for doped and co-doped ZnO thin films.

✓ CHAPTER II: Thin films deposition techniques and characterization methods

The second chapter describes the spray pyrolysis technique. Furthermore, we explain the methodologies utilized in this study to characterize ZnO films (such as structural, optical, and electrical studies).

✓ CHAPTER III: Experimental result and discussion

This chapter also summarizes the numerous experimental results obtained (structural, optical, and electrical properties) from the thin ACZO films made utilizing the aerosol decomposition process, as well as their discussion and comparison.

Finally, we will conclude our work with a general conclusion in which we identify all the significant results that we have obtained during this work .

References

- [1] El Hichou, A., Addou, M., Bougrine, A., Dounia, R., Ebothé, J., Troyon, M., & Amrani, M. (2004). Cathodoluminescence properties of undoped and Al-doped ZnO thin films deposited on glass substrate by spray pyrolysis. Materials chemistry and physics, 83(1), 43-47.
- [2] Nasiri, M., & Rozati, S. M. (2018). Muscovite mica as a flexible substrate for transparent conductive AZO thin films deposited by spray pyrolysis. Materials Science in Semiconductor Processing, 81, 38-43.
- [3] Mohamedi, M., Challali, F., Touam, T., Mendil, D., Ouhenia, S., Souici, A. H., ... & Chelouche, A. (2022). Role of substrate and annealing on microstructural, optoelectronic and luminescence properties of RF magnetron sputtered AZO thin films in confocal configuration. Journal of Luminescence, 244, 118739.
- [4] Janotti, A., & Van de Walle, C. G. (2009). Fundamentals of zinc oxide as a semiconductor. Reports on progress in physics, 72(12), 126501.
- [5] Look, D. C. (2001). Recent advances in ZnO materials and devices. Materials science and engineering: B, 80(1-3), 383-387.
- [6] Wei, Y. Y., Hou, D. L., Zhao, R. B., Zhou, Z. Z., Zhen, C. M., & Tang, G. D. (2008). Structural and magnetic properties of cobalt and aluminum co-doped ZnO powders. Advanced Materials Research, 47, 600-603.
- [7] Dang, W. L., Fu, Y. Q., Luo, J. K., Flewitt, A. J., & Milne, W. I. (2007). Deposition and characterization of sputtered ZnO films. Superlattices and Microstructures, 42(1-6), 89-93.
- [8] Ilican, S., Caglar, Y., & Caglar, M. (2008). Preparation and characterization of ZnO thin films deposited by sol-gel spin coating method. Journal of optoelectronics and advanced materials, 10(10), 2578-2583.
- [9] Craciun, V., Elders, J., Gardeniers, J. G. E., & Boyd, I. W. (1994). Characteristics of high quality ZnO thin films deposited by pulsed laser deposition. Applied physics letters, 65(23), 2963-2965.

- [10] wang, L., Zhang, X., Zhao, S., Zhou, G., Zhou, Y., & Qi, J. (2005). Synthesis of well-aligned ZnO nanowires by simple physical vapor deposition on c-oriented ZnO thin films without catalysts or additives. Applied Physics Letters, 86(1), 013102.
- [11] Khediri, F. (2022). Etude expérimental des propriétés physiques des couches minces de ZnO (Doctoral dissertation, Université Echahid Cheikh Larbi-Tebessi-Tébessa).

Chapter I: Overview of TCOs and ZnO

This chapter focuses on the theoretical research aspect, introducing transparent conductive oxides (TCOs) and zinc oxide (ZnO) with an emphasis on their key physical properties, including crystal structure, electrical behavior, and optical characteristics. The chapter also reviews the most important practical applications of ZnO, in addition to previous studies on ZnO doping with various elements, whether single or co-doping, aiming to enhance its functional properties.

I.1Transparent conductive oxide (TCO)

I.1.1Definition of TCO

Transparent conductive oxides (TCOs) are binary or ternary inorganic compounds composed of one or two metallic elements, which simultaneously exhibit high optical transparency and good electrical conductivity. These materials have a wide optical bandgap (Eg) of more than 3 eV resulting in low resistivity (as low as 10^{-4} cm) and extinction coefficients (k) in the visible range (VIS) of less than 0.0001[1].

The formation of non-stoichiometric oxides or the intentional introduction of suitable dopants can lead to an exceptional combination of electrical conductivity and optical transparency properties that are typically incompatible in stoichiometric, undoped oxides.[2] Their discovery dates back to the early 20th century, when Bädeker observed that thin films of cadmium oxide (CdO) deposited in a glow discharge chamber were both conductive and transparent. This first discovery paved the way for a field of research that is still relevant a century later.[3]

Many TCO materials were subsequently developed, including In_2O_3 , SnO_2 , ZnO:, Cd_2SnO_4 , Cd_2SnO_2 , $In_2O_2:Sn(ITO)$, ZnO: Al, etc. Obtaining these materials, which provide a good compromise between transparency to visible light and

electrical conductivity, is a major industrial challenge [4]. These transparent conductive oxides are widely used materials because many applications need to combine optical transparency with electrical conductivity. Some of these applications are listed below:

Ecrans plats, heat-reflective objects, such as heat-reflective windows and mirrors, etc. Electromagnetic windows and mirrors, electric mirrors, touch screen controls, electromagnetic shielding, electrostatic charge dissipation, solar cells: The first point of contact through which light must pass to enter the cell. A unique TCO is selected for each of these applications based on the manufacturing requirements and other properties (stability against specific elements, etc.) required by the application [5].

I.1.2. Properties of TCO

I.1.2.1. Electrical properties

The electrical properties of TCOs are governed by the physical characteristics of wide band gap semiconductors (Eg > 3 eV). The electrical conductivity (σ), expressed in S·cm⁻¹ or equivalently (Ω ·cm) ⁻¹, is determined by the charge carrier density (n, in cm⁻³), the charge carrier mobility (μ , in cm²·V⁻¹·s⁻¹), and the elementary charge of the electron (q, in coulombs). The electrical resistivity (ρ) is defined as the inverse of conductivity and is expressed in Ω ·cm [6].

$$\sigma = q n_v \mu = \frac{1}{\rho} \tag{I.1}$$

I.1.2.2. Optical Properties:

TCOs are characterized by the presence of an optical window that spans the entire visible spectrum. Optical transmission is defined as the ratio between the intensity of the incident light and the intensity of the light transmitted through the material under investigation.[7] These activities generate additional characteristics used to analyze optical qualities. They are called absorbance, reflectance, and transmittance. respectively. A medium's reflectance 'R' is the ratio of flux reflected to flux incident. Transmittance 'T' is the quantity of flux transmitted by the medium, normalized by the amount of flux incident on the same medium. Absorbance 'A' refers to any flux that is not reflected or transmitted. The law of conservation of energy states that the total of three parameters equals one unit.[8]

$$R + T + \alpha = 1 \tag{I.2}$$

α: absorption coefficient

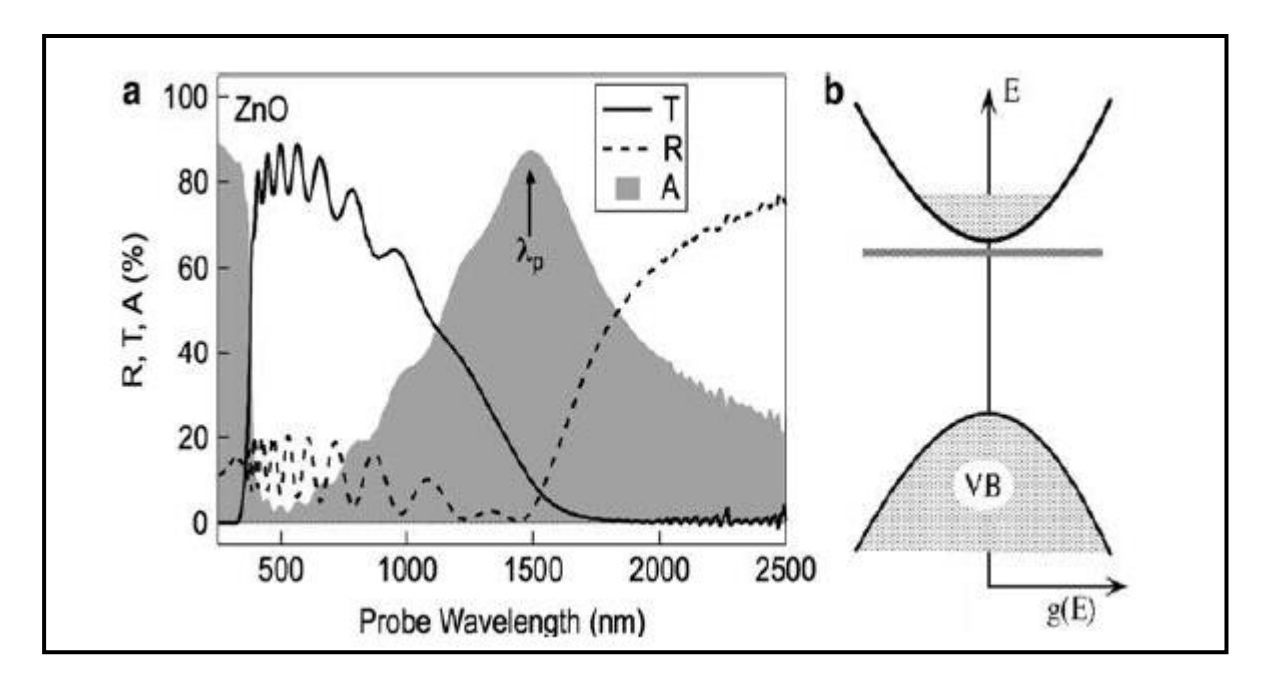


Figure I-1: Optical spectra of typical (ZnO) transparent conductor (left side) and schematic electronic structure of conventional TCO materials (right side) conduction band [9]

Transparent conductive oxides (TCOs) possess an optical window that spans the entire visible spectrum. As illustrated in Figure (I-1), their optical behavior can be divided into three spectral regions.

In the **short-wavelength range** ($\lambda < \lambda g$), corresponding to the near-ultraviolet region, optical absorption is primarily due to interband (band-to-band) transitions, where incident photons with energies equal to or greater than the band gap excite electrons from the valence band to the conduction band.

In the **intermediate region** ($\lambda g < \lambda < \lambda p$), which corresponds to the visible range, the material exhibits high transparency, as photon energies are insufficient for band-to-band excitation and are not significantly absorbed by free carriers. Finally, in the **long-wavelength range** ($\lambda > \lambda p$), corresponding to the near-infrared region, incident radiation is reflected by free electrons in the conduction band. This phenomenon can be interpreted using classical Drude free-electron theory. Plasma oscillates at a natural frequency ωp , called the resonance frequency or plasma frequency, corresponding to a characteristic wavelength λp . At this wavelength, part of the incident radiation is absorbed by the thin film due to the presence of

free electrons in the material, a phenomenon influenced by their concentration and motion [10].

I.1.3. Criteria for Choosing TCOs

The most suitable transparent conductive oxides (TCOs) are selected based on their high electrical conductivity and excellent optical transparency as summarized in Table 1, as well as additional factors such as physical and chemical stability, plasma wavelength, film thickness, deposition temperature, toxicity, and cost, [11].

Furthermore, the **figure of merit** proposed by Haacke in 1976 serves as a key criterion for evaluating transparent semiconductor materials. It is defined as the ratio of optical transmittance to the sheet resistance of the TCO layer and is expressed in units of Ω^{-1} [12]

$$\phi_{Tc} = \frac{T^{10}}{R_s} \tag{1.3}$$

Table (I-1): Minimum required properties of TCOs [11]

Parameters	Transparent Conductive Materials
Band gap	>3.1eV (380nm)
Transparency at 550nm	>90% (for n-type) and >85% (for p-type)
Resistivity	10 ⁴ cm (for n-type) and 10 ³ cm (for p-type)
Carrier Concentration	$>10^{20} cm^{-3}$ (for n-type) and $>10^{18} cm^{-3}$ (for p-type)
Mobility	$>40cm^2(Vs)^{-1}$ (for n-type) and $>20cm^2(Vs)^{-1}$ (for p-type)
Sheet resistance	≤10k /square (for 20nm thickness)

I.2. Zinc Oxide (ZnO)

I.2.1. The Choice of ZnO

ZnO is attracting a lot of interest for its applications in optoelectronic devices, including UV-blue LEDs and lasers. Its main properties include [13]:

- High exciton energy (60 meV), ideal for UV laser diodes.
- Transparency in the visible and near infrared.
- High hardness and thermal stability.
- Low cost, natural abundance and non-toxicity.

- A two-dimensional growth favored on substrates such as sapphire.
- The possibility of high doping with low resistivity.
- Good compatibility with other active semiconductors.
- The manufacture of TCO films on large surfaces by sputtering.
- Interesting characteristics even at low deposition temperatures.
- Thanks to these properties, ZnO is positioned as a key material for the next generation of optoelectronic devices.
- The figure of merit $(7 \Omega^{-1})[12]$

I.2.2. Definition of Zinc Oxide

Zinc oxide is an important material in the electronics industry, classified as a II-VI oxide semiconductor with the chemical formula ZnO [14]. It is insoluble in water but dissolves in acids and alcohols. Its melting point exceeds 2250 K, and its density reaches 5675 kg/m³.[15]

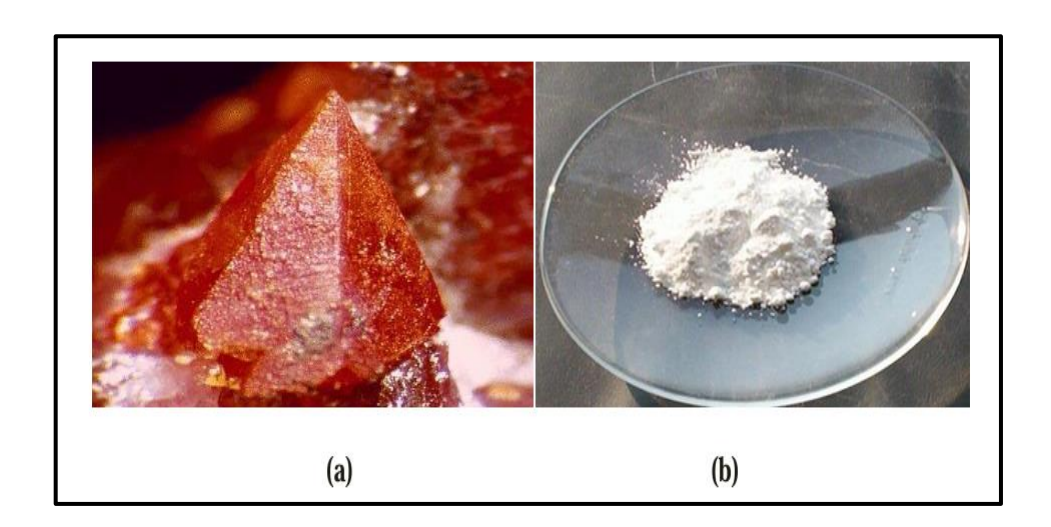


Figure I-2: Solid zinc oxide in natural form (a) and in the form of a white powder called "white zinc" (b) [16]

I.2.3. Zinc Oxide Properties

I.2.3.1. Structural properties

Zinc oxide (ZnO) crystallizes in three main crystal structures: hexagonal wurtzite, cubic zinc blende, and cubic rocksalt shown in Figure (I-3) [17]. Among these, the wurtzite structure is the most thermodynamically stable and commonly observed under ambient conditions.

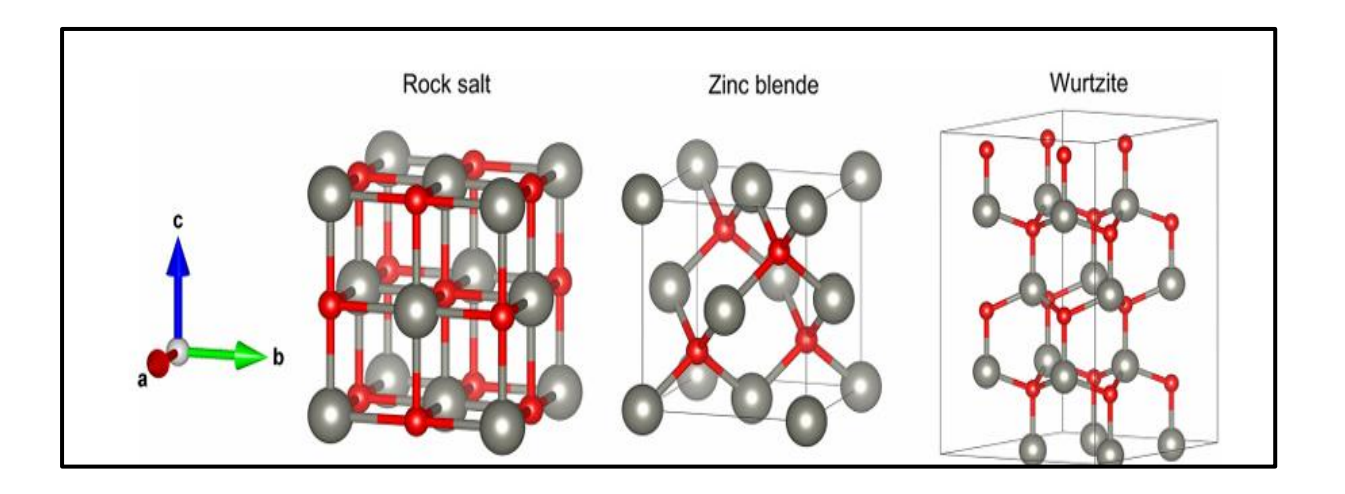


Figure I-3: The ZnO crystal structures, rocksalt, zinc blend, wurtzite

The zinc blende phase can only be stabilized when ZnO is grown on cubic substrates, while the rocksalt structure appears only under high pressures, approximately 10 GPa. The wurtzite structure is characterized by tetrahedral coordination, where each Zn^{2+} ion is surrounded by four O^{2-} ions, and vice versa. This arrangement results in a non-centrosymmetric structure, which gives ZnO unique physical properties such as piezoelectricity and spontaneous polarization. These properties significantly influence crystal growth, etching behavior, and defect formation [17,18]. The ideal wurtzite structure is defined by the following lattice parameters: (a = 3.25 Å, c = 5.21 Å and Ideal c/a ratio = 1.63)

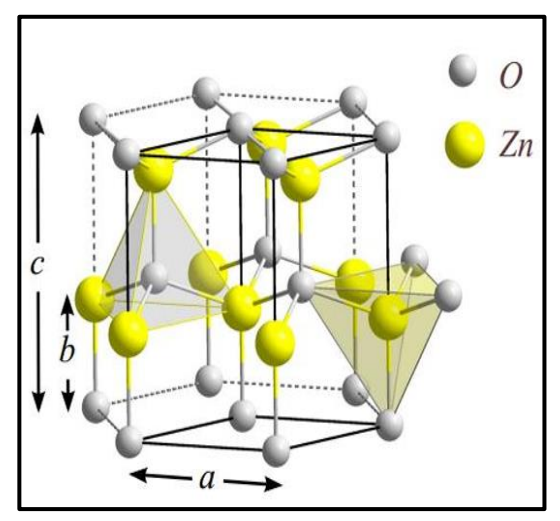


Figure I-4: Wurtzite Structure of Zinc Oxide [16]

I.2.3.2. Electrical Properties

Zinc oxide (ZnO) is an n-type semiconductor whose electrical resistivity can be controlled through doping, either by introducing excess zinc atoms into interstitial sites or

by creating oxygen vacancies. Both mechanisms increase the concentration of free electrons, there by reducing resistivity. The resistivity of ZnO thin films is highly sensitive to preparation conditions and thermal treatment, with reported values ranging from 10^{-4} to 10^{12} $\Omega \cdot \text{cm}$. [19]

Deposition temperature has a significant influence on the material's properties: studies have shown that increasing the annealing temperature from 160 °C to 300 °C enhances electron mobility and crystallite size; however, further temperature increases may cause degradation. ZnO possesses a wide, tunable bandgap centered around 3.3 eV, varying between 2.88 eV and 3.45 eV depending on the synthesis method and dopants used [20].

Its properties can be improved by modifying its chemical composition or doping with group III elements or halide ions like F^- and Cl^- . Aluminum doping enhances ZnO's performance by reducing interstitial zinc and limiting oxygen adsorption, allowing for very low resistivity at high doping levels (up to 10^{20} atoms/cm³). At the atomic level, ZnO consists of ionic bonding between Zn and O, where oxygen's 2p orbitals form the valence band and zinc's 4s orbitals form the conduction band. ZnO has a direct band gap, with both conduction band minimum and valence band maximum located at the Γ point, and stoichiometric ZnO behaves as an insulator [21,22].

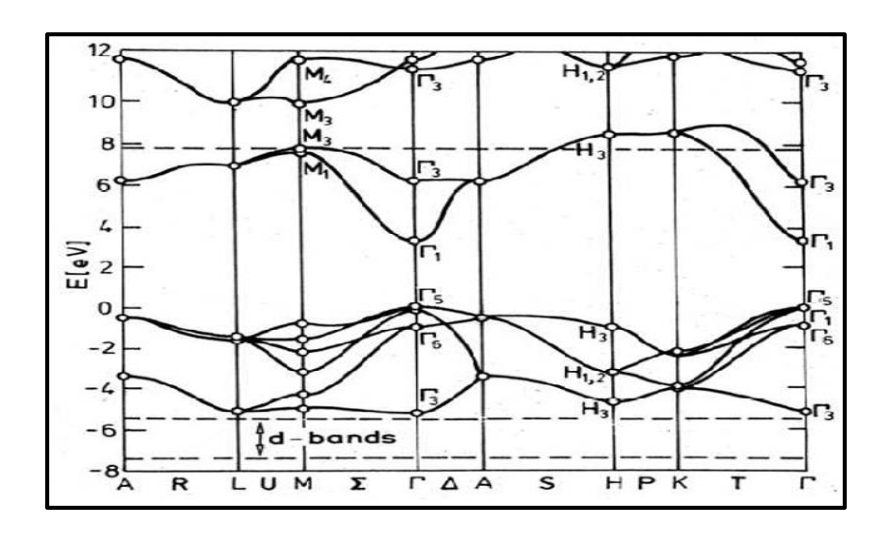


Figure I-5: Structure de bande mesurée pour l'oxyde de zinc en symétrie Wurtzite [21]

I.2.3.3. Optical Properties

The optical absorption and refraction coefficients of zinc oxide (ZnO) are strongly dependent on its structural and chemical quality. In its high-purity form, ZnO exhibits a transmittance of up to 80% in the visible spectrum, with a refractive index of approximately 2.0. Its high absorption coefficient near 3.3 eV places ZnO among the class of transparent conducting oxides (TCOs) [23]

ZnO is also known for its pronounced ultraviolet emission centered around 367 nm (3.37 eV), which arises from near band edge (NBE) recombination involving free or bound excitons. In addition, ZnO exhibits broad visible emission in the 400–600 nm range, typically attributed to intrinsic defects that influence both optical and electronic behavior. The most common structural defects include oxygen and zinc vacancies, interstitials atoms occupying non-ideal lattice sites [24].

Table (**I-2**): Optical properties of zinc oxide (ZnO) thin films prepared by different deposition methods

Method	Eg (eV)	T (%)	Ref
Sol – gel	3.312-3.381	93	[25]
Spin coating			
simple method	3.23-3.29		[26]
chemical vapor	3.34-3.4	90	[27]
chemical vapor	3.29-3.44	~100	[28]
MOCVD	3.27-3.44	93	[29]
Spray Pyrolysis	3.25-3.30	85	[30]

I.2.4. Doping of ZnO

Doping ZnO presents significant challenges, especially in achieving p-type conductivity. Although group I elements (such as Li, Na, and K) and group Ib elements (such as Cu and Ag) act as acceptors, they are usually deep acceptors with high ionization energies, making them ineffective at room temperature. Additionally, at high concentrations, some of these elements can act as donors, compensating for the acceptors' effects. Due to the high

incorporation of cations in hydrothermally grown samples, these materials exhibit high resistivity, making n-type doping difficult. To achieve more efficient p-type doping, group V elements (such as N, P, and As) are used to replace oxygen in the crystal lattice [31].

However, their solubility is low, and the resulting hole density is significantly lower than the incorporated acceptor atoms. This leads to the formation of complexes or defect states that may act as donors, reducing doping efficiency. Recent research has proposed codoping methods, such as combining two different acceptors or mixing donors and acceptors to achieve better stability. [32]

For n-type doping in ZnO, group III elements (such as Al, Ga, and In) are considered effective donor dopants when they substitute zinc atoms in the cation sublattice. This substitution leads to high free electron concentrations, often reaching up to 10^{20} cm⁻³, resulting in the formation of a degenerate electron gas that significantly affects the material's optical and electrical properties. Group VII elements, when incorporated at the oxygen (anion) site, may also act as donors. However, this doping strategy remains relatively unexplored in the case of ZnO. Additionally, hydrogen in ZnO consistently behaves as a shallow donor, which partly explains the intrinsic n-type conductivity commonly observed in undoped ZnO samples [33].

Table (I.3): Summary of different doped ZnO thin films as transparent conductors

Dopant	Methods	Resistivity $(\Omega.cm)$	Band gap (eV)	Transmittance (%)	Ref
В	dip coating	1.25×10^4	3.27-3.30		[34]
Mg	Sol-gel			90	[35]
Na	Sol-gel		3.15-3.17	>85	[36]
Fe	Spray Pyrolysis	2.9×10^{-2}	3.3	45-70	[37]

I.2.5. Co-doped ZnO

I.2.5.1. Scope of co-doped ZnO

When ZnO is doped with cations, resistivity decreases due to the increase in donor electrons. However, beyond the solubility limit of the dopant, resistivity starts to increase again. Therefore, co-doping (dual doping) with an additional cation or anion alongside the primary cation dopant has been adopted to enhance electrical and crystalline properties. Cation-cation co-doping aims to increase the solubility of dopants, while cation-anion co-doping provides free charge carriers from both the cation and anion. Fluorine (F) is preferred for co-doping as it can substitute oxygen in the ZnO lattice, introducing extra electrons into the conduction band (CB) and reducing scattering. This enhances carrier mobility and improves [38]

Table (**I-4**): Summarizes the results of these trials, highlighting variances in the co-doping technique.

Co-Dopant	Methods	Resistivity	Transmittance	Ref
		$(\Omega.cm)$	(%)	
Zr/F (ZFZO)	Sol-gel	3.8×10^{-3}	>85	[39]
In/Ga IGZO	RF sputtering	10-2	90	[40]
Al/Ga AGZO	Sol-gel Dip coating	18	>85	[41]
Ti/Ga TGZO	magnetron sputtering	6.715×10^{-4}	~88.24	[42]
In/F IFZO	Spray pyrolysed	2×10^{-3}	80	[43]

I.2.5.2. Co, Al Co-doped ZnO (ACZO)

The term "ACZO" is a strategic abbreviation that high lights the key elements in this doped material: "A" for aluminum, "C" for cobalt, "Z" from zinc, and "O" representing oxide. This naming reflects the composite nature of the material.

Al and Co co-doped ZnO (ACZO) introduces an innovative strategy for modifying ZnO properties by incorporating aluminum (Al) and cobalt (Co) into its crystal structure. This co-doping approach is designed to improve electrical conductivity and optical performance, making it highly suitable for applications in electronics and photonics. [44,45]

Table (I-5): Al and	d Co doped and	co-doped ZnO
---------------------	----------------	--------------

Dopant Co-Dopant	methods	T (%)	Eg(eV)	Resistivity $(\Omega.cm)$	Ref
Al	Spray Pyrolysis	90	3.30-3.55		[46]
	Sol-gel	79	3.30-3.32	7.561×10^{-3}	[47]
	Dip coating	90	3.29	2.1×10^{-2}	[48]
	AACVD	38-75	3.17-2.79		[49]
Со	Sol-gel	75	3.68-3.77		[50]
	Sol-gel	~90	3.22-2.84		[51]
ACZO	Sol-gel			~10 ⁷	[52]
ACZO	Electrospray	~80	3.33		[44]

I.2.6. Major applications of zinc oxide

Zinc oxide is a good semiconductor with potential applications in photovoltaics, electroluminescent diodes, transparent conductors, capacitors, and spintronics due to its electrical, optical, and magnetic properties.

a) Transparent Conductive Oxide and Solar Cells:

Zinc oxide (ZnO) is a material from the oxide family that, in addition to being transparent (as it does not absorb photons with energy lower than its band gap, making it transparent to visible light), can become an n-type conductor if it contains an excess of

electrons in its crystalline structure. This excess of electrons can be generated either by structural defects causing an imbalance in the oxide's stoichiometry or through doping.

These materials are known as Transparent Conductive Oxides (TCOs). Thin ZnO films with good conductivity and high transparency in the visible spectrum have been used as transparent electrodes in solar cells. These cells are semiconductor based systems capable of converting solar energy into electrical energy through the photovoltaic effect, where the material absorbs photon energy to excite charge carriers from the valence band to the conduction band. In this application, ZnO can serve as a transparent electrode in the upper "contact" layer, allowing electric current to pass through while still transmitting light. Additionally, ZnO can function as an n-type semiconductor, increasing the effective surface area for light interaction, thereby improving solar cell efficiency. Several studies, including those conducted by Fahmi Machdaet al, have reported on the fabrication and characterization of aluminum-doped ZnO thin films as transparent conductive oxides for solar cells. [53]

b) Light-Emitting Diodes (LEDs)

ZnO/Si light-emitting diodes (LEDs) were fabricated by depositing nanoscale ZnO onto single-crystal silicon using radio frequency (RF) magnetron sputtering. ZnO is considered a promising material for optoelectronic applications due to its environmental friendliness, ease of preparation, excellent stability, and high exciton binding energy (60 meV). Various methods have been used to synthesize ZnO with different morphologies, including chemical bath deposition, vapor, liquid and solid (VLS) method, magnetron sputtering, and metal organic chemical vapor deposition (MOCVD).

In the field of LEDs, significant research efforts have focused on utilizing ZnO to produce blue or violet emissions in the 350–420 nm range. Some researchers have combined the blue or violet emission from ZnO's bandgap with green emission caused by structural defects to generate white light. This method eliminates the need for separate RGB LEDs and avoids issues related to mismatched emission layers and self-absorption during color mixing and conversion. However, this direct white light generation approach is highly sensitive to preparation conditions.[54]

c) UV Photodetection and Protection

Radiation detectors are information converters. A photodetector absorbs an optical signal and converts it into an electrical signal. A photoconductive cell consists of a photosensitive semiconductor (ZnO) placed between two electrodes across which a potential difference is applied. When the surface of the photoconductor is illuminated by photons with sufficient energy (UV), the density of free charges increases due to the photoelectric effect, resulting in a measurable current. Its ability to absorb UV light makes zinc oxide a prime candidate for use in sunscreens. Many metal oxide materials are used in the formulation of cosmetic products (cream, foundation, nail polish, etc.), therapeutic products (hygiene and care products), or preventive products (sunscreen). Zinc oxide (ZnO) and titanium dioxide (TiO₂) are commonly used in sunscreens.[55]

d) Gas Sensors

With the advancement of industry and science, solid-state gas sensors have become important for detecting toxic and flammable gases, playing a crucial role in personal safety, environmental monitoring, and industrial processes. These sensors are known for their low cost and lightweight properties. Among the materials used, metal oxide semiconductors such as ZnO, SnO₂, and TiO₂ have gained significant attention due to their effectiveness and gas sensing capabilities. In recent years, ZnO has emerged as a key gas sensing material because of its wide bandgap energy (3.4 eV) and its versatility in forming various nanostructures such as nanoparticles, nanowires, and thin films. These nanostructures increase the surface active sites density, thereby improving sensitivity. Furthermore, doping ZnO with elements like indium enhances its gas sensing properties by inducing structural and morphological changes that improve sensor performance. The current study aims to develop low-cost, effective acetylene gas sensors using indium-doped ZnO thin films with varying doping concentrations to enhance sensitivity and overall performance [56]

e) Photocatalysts

It is expected that the issue of water pollution caused by textile dyes due to industrial growth and population increase will gain increased attention, leading to a heightened focus on wastewater treatment. Photocatalytic treatment is considered one of the most important methods used, employing semiconductors such as TiO₂ and ZnO because of their distinctive physical and chemical properties. TiO₂ is characterized by its high ultraviolet light absorption and chemical stability; however, it suffers from drawbacks such as a wide band gap and a high recombination rate of electron-hole pairs. On the other hand, ZnO exhibits good photocatalytic activity, a stable structure, and a large band gap, but it also faces issues like photo-corrosion and a high recombination rate. To overcome these limitations, research has focused on enhancing the performance of TiO₂ and ZnO by doping them with metal elements such as copper, silver, cadmium, and iron, which helps reduce the recombination rate and improve photocatalytic efficiency [57].

f) Spin-Based Electronics (Spintronics)

The rapid advancement in microelectronics and optoelectronics primarily relies on the electric charge of electrons. However, another fundamental property of electrons, their spin, plays a crucial role in information storage within magnetic materials. In traditional electronic systems, transistors made of semiconductor materials transmit information through charge currents in conduction channels, enabling computation and dataprocessing. On the other hand, data storage is carried out using magnetic components, where information is encoded through the magnetization of magnetic materials, specifically through the spin orientation of electrons in the d-layer. However, electron conductivity properties are not utilized in this process, and spin properties are not used in traditional processing and computing units. Spintronics has led to a technological revolution with significant applications, most notably in hard disk data reading technologies. One effective method to achieve high spin polarization at room temperature is doping non-magnetic semiconductor oxides withmagnetic ions, leading to the formation of Diluted Magnetic Semiconductors (DMS). Among the most widely used materials in this field are titanium dioxide (TiO₂) and cobalt-doped zinc oxide (Co-doped ZnO) [55].

Refereces

- [1] CastaÃeda, L. (2022). Review of Conducting Oxides Semiconductors in Thin Solid Films. Biomedical Journal of Scientific & Technical Research, 41(1), 32261-32270.
- [2] Afre, R. A., Sharma, N., Sharon, M., & Sharon, M. (2018). Transparent conducting oxide films for various applications: A review. Reviews on advanced materials science, 53(1), 79-89.
- [3] Li, K., Willis, J., Kavanagh, S. R., & Scanlon, D. O. (2024). Computational prediction of an antimony-based n-type transparent conducting oxide: F-doped Sb2O5. Chemistry of Materials, 36(6), 2907-2916.
- [4] Ynineb, F. (2010). Contribution à l'élaboration de couches minces d'Oxydes Transparents Conducteurs (TCO). mémoire de Magister en physique, univ-Mentouri-Constantine.
- [5] Bouhssira, N. (2013). Élaboration des films minces d'oxyde de zinc par évaporation et par pulvérisation magnétron et étude de leurs propriétés [Thèse de doctorat, Université Constantine 1].
- [6] Bouaraba, F. (2019). Etude de l'effet de vieillissement sur les propriétés structurales et optoélectroniques des couches minces des oxydes transparents conducteurs (TCO) (Doctoral dissertation, Université Mouloud Mammeri).
- [7] Garnier, J. (2009). Elaboration de couches minces d'oxydes transparents et conducteurs par spray CVD assiste par radiation infrarouge pour applications photovoltaïques (Doctoral dissertation, Paris, ENSAM)
- [8] Adedokun, O. (2018). Review on Transparent Conductive Oxides Thin Films deposited by Sol-gel spin coating technique. International Journal of Engineering Science and Application, 2(3), 88-97.
- [9] Ginley, D. S., & Perkins, J. D. (2010). Transparent conductors. In Handbook of transparent conductors (pp. 1-25). Boston, MA: Springer US.

- [10] Touati Tliba, M. (2019). Étude des propriétés optiques et électroniques des couches minces de ZnO dopé et non dopé: élaboration et application [Thèse de doctorat de 3° cycle, Université Kasdi Merbah Ouargla]).
- [11] Khan, A. (2011). Synthesis of Strontium Cuprate (SrCu2O2) by MOCVD as a P-type Transparent Conducting Oxide Thin Film (Doctoral dissertation, Institut National Polytechnique de Grenoble-INPG; Université de Grenoble).
- [12] Khenfer, H. (2020). دراسة الخصائص البصرية لغشاء رقيق من أوكسيد الزنك النقي (ZnO) دراسة الخصائص البصرية لغشاء رقيق التحلل الحراري [مذكرة ماستر، جامعة قاصدي مرباح ورقلة].
- [13] Bahtoun, H. (2023). Élaboration et caractérisation par différentes techniques de couches minces d'oxydes métalliques utilisables comme capteurs et pour la photocatalyse [Thèse de doctorat de 3^e cycle, Université Larbi Ben M'hidi, Oum El Bouaghi].
- [14] Dahnoun, M. (2020). Preparation and characterization of titanium dioxide and zinc oxide thin films via Sol-Gel (spin coating) technique for optoelectronic applications [Doctoral dissertation, University Mohamed Khider of Biskra]. Faculty of Exact Sciences and Nature and Life, Department of Matter Sciences.
- [15] Kouidri, N. (2019). Contribution à l'étude de couches minces d'oxydes transparents conducteurs à base de zinc et cobalt par spray pneumatique (Doctoral dissertation, University of Mohamed Khider, BISKRA).
- [16] Hadj Chikh, M. (2024). Étude des propriétés de photoluminescence et morphologiques des couches minces de ZnO dopées aux métaux de transition (TM = Mn, Ni): une étude comparative [Mémoire de master, Université Belhadj Bouchaib d'Aïn Témouchent]
- [17] Han, Y., Guo, J., Luo, Q., & Ma, C. Q. (2023). Solution-Processable Zinc Oxide for Printed Photovoltaics: Progress, Challenges, and Prospect. Advanced Energy and Sustainability Research, 4(10), 2200179.
- [18] Othmane, M. (2010). dépôt et caractérisation des couches minces d'oxyde de zinc par spray pyrolyse ultrasonique (Doctoral dissertation, Université Mohamed Khider-Biskra).
- [19] López-Mena, E. R., Jiménez-Sandoval, S. J., & Jiménez-Sandoval, O. (2021). Samarium-doped ZnO thin films synthesized by Sol-gel: Structural, optical and electrical properties. Materials Science in Semiconductor Processing, 126, 105648.

- [20] Nafees, M., Liaqut, W., Ali, S., & Shafique, M. A. (2013). Synthesis of ZnO/Al: ZnO nanomaterial: structural and band gap variation in ZnO nanomaterial by Al doping. Applied Nanoscience, 3, 49-55.
- [21] Baka, O. (2015). Dopage électrochimique des oxydes métalliques : Applications aux photovoltaïques [Thèse de doctorat de 3^e cycle, Université Sétif-1]
- [22] Diouf, A. A. (2017). Etude des propriétés optiques de photoluminescence et de réflectivité de couches minces de ZnO épitaxiées sous jets moleculaires et détermination á l'aide du modèle d'Ising des propriétés ferromagnétiques de nanomatériaux de ZnO dopés par des impuretés magnétiques (Doctoral dissertation, Cheikh Anta Diop University).
- [23] Latif, A. (2024). Elaboration of pure and doped ZnO powders with the sol gel method (Doctoral dissertation, Université Mohamed Khider (Biskra-Algérie)).
- [24] Hakkoum, H. (2022). *Design of a photodiode based on NiO/ZnO heterojunction* (Doctoral dissertation, Université de mohamed kheider biskra).
- [25] Caglar, M., Ilican, S., Caglar, Y., & Yakuphanoglu, F. (2009). Electrical conductivity and optical properties of ZnO nanostructured thin film. *Applied surface science*, 255(8), 4491-4496.
- [26] Zandi, S., Kameli, P., Salamati, H., Ahmadvand, H., & Hakimi, M. (2011). Microstructure and optical properties of ZnO nanoparticles prepared by a simple method. *Physica B: Condensed Matter*, 406(17), 3215–3218
- [27] Malandrino, G., Blandino, M., Fragala, M. E., Losurdo, M., & Bruno, G. (2008). Relationship between nanostructure and optical properties of ZnO thin films. The Journal of Physical Chemistry C, 112(26), 9595-9599.
- [28] Tan, S. T., Chen, B. J., Sun, X. W., Hu, X., Zhang, X. H., & Chua, S. J. (2005). Properties of polycrystalline ZnO thin films by metal organic chemical vapor deposition. Journal of crystal growth, 281(2-4), 571-576.
- [29] Myong, S. Y., & Lim, K. S. (2005). Improvement of electrical and optical properties of ZnO thin films prepared by MOCVD using UV light irradiation and in situ H2 post-treatment. Solar energy materials and solar cells, 86(1), 105-112.

- [30] Karaköse, E., & Çolak, H. (2017). Structural and optical properties of ZnO nanorods prepared by spray pyrolysis method. *Energy*, *140*, 92–97
- [31] Taibarei, N. O., Kytin, V. G., Konstantinova, E. A., Kulbachinskii, V. A., Shalygina, O. A., Pavlikov, A. V., ... & Baranov, A. N. (2022). Doping nature of group V elements in ZnO single crystals grown from melts at high pressure. *Crystal Growth & Design*, 22(4), 2452-2461.
- [32] Yang, X., & Xue, M. (2021). First-principle investigation of Li–N dual-acceptor codoping for p type ZnO: The effect of electric fields. Physica B: Condensed Matter, 620, 413271.
- [33] Klingshirn, C. (2007). ZnO: material, physics and applications. ChemPhysChem, 8(6), 782-803.
- [34] Senol, S. D., Ozturk, O., & Terzioğlu, C. (2015). Effect of boron doping on the structural, optical and electrical properties of ZnO nanoparticles produced by the hydrothermal method. Ceramics International, 41(9), 11194-11201.
- [35] Mahroug, A., Mari, B., Mollar, M., Boudjadar, I., Guerbous, L., Henni, A., & Selmi, N. (2019). Studies on structural, surface morphological, optical, luminescence and Uv photodetection properties of sol–gel Mg-doped ZnO thin films. Surface Review and Letters, 26(03), 1850167.
- [36] Tong, F., Zhao, Y., & Wang, M.-H. (2019). Microstructure and optical properties of Na-doped ZnO system, synthesized by the sol–gel method. Canadian Journal of Chemistry, 97(4), 254–258.
- [37] Abdelmalek, N., Hadjeris, L., Herissi, L., Rahmane, S., & Moualkia, H. (2014). Structural, Optical and Electrical Properties of ZnO: Fe Thin Films Grown by Spray Pyrolysis. Journal of new technology and materials, 4(2), 47-50.
- [38] Mallick, A., & Basak, D. (2018). Revisiting the electrical and optical transmission properties of co-doped ZnO thin films as n-type TCOs. Progress in Materials Science, 96, 86-110.

- [39] Ravichandran, K., Rajkumar, P. V., Sakthivel, B., Manoharan, C., Ravidhas, C., & Chinnappa, L. (2016). Effect of Zr+ F doping and vacuum annealing on the transparent conducting properties of ZnO thin films. Materials Research Innovations, 20(2), 106-111.
- [40] Shi, J., Dong, C., Dai, W., Wu, J., Chen, Y., & Zhan, R. (2013). The influence of RF power on the electrical properties of sputtered amorphous In—Ga—Zn—O thin films and devices. *Journal of Semiconductors*, *34*(8), 084003..
- [41] Ebrahimifard, R., Golobostanfard, M. R., & Abdizadeh, H. (2014). Sol–gel derived Al and Ga co-doped ZnO thin films: An optoelectronic study. *Applied Surface Science*, 290, 252-259.
- [42] Lu, Z., Long, L., Zhong, Z., & Lan, C. (2016). Structural characterization and optoelectrical properties of Ti–Ga co-doped ZnO thin films prepared by magnetron sputtering. Journal of Materials Science: Materials in Electronics, 27, 2875-2884.
- [43] Vimalkumar, T. V., Poornima, N., Jinesh, K. B., Kartha, C. S., & Vijayakumar, K. P. (2011). On single doping and co-doping of spray pyrolysed ZnO films: Structural, electrical and optical characterisation. Applied Surface Science, 257(20), 8334-8340.
- [44] Marinov, G., Georgieva, B., Vasileva, M., & Babeva, T. (2023). Study of structure, morphology and optical properties of cobalt-doped and Co/Al-co-doped ZnO thin films deposited by electrospray method. Applied Sciences, 13(17), 9611.
- [45] Winarsih, S., Jatmika, J., Roza, L., Risdiana, R., & Watanabe, I. (2024). Effect of cobalt and aluminum doping on the structural and magnetic properties of zinc oxide nanoparticles. AIP Advances, 14(4), 045044.
- [46] Kaid, M. A., & Ashour, A. (2007). Preparation of ZnO-doped Al films by spray pyrolysis technique. Applied surface science, 253(6), 3029-3033.
- [47] Chen, J., Chen, D., He, J., Zhang, S., & Chen, Z. (2009). The microstructure, optical, and electrical properties of sol–gel-derived Sc-doped and Al–Sc co-doped ZnO thin films. Applied Surface Science, 255(23), 9413-9419.
- [48] Manjakkal, L., Packia Selvam, I., Potty, S. N., & Shinde, R. S. (2017). Electrical and optical properties of aluminium doped zinc oxide transparent conducting oxide films prepared by dip coating technique. Microelectronics International, 34(1), 1-8.

- [49] Basit, M., Shah, N., Ali, S., & Zia, A. (2014). Cobalt doping effects on zinc oxide transparent conducting thin films. World Applied Sciences Journal, 32(8), 1664-1670.
- [50] Joshi, S., & Leela, S. (2021). Studies on structural and optical properties of Cobalt doped ZnO thin films prepared by Sol-gel spin coating technique. Materials Today: Proceedings, 43, 3166-3168.
- [51] Xian, F. L., Xu, L. H., Wang, X. X., & Li, X. Y. (2012). Crystallographic, optical and magnetic properties of Co-doped ZnO thin films synthesized by sol gel route. Crystal Research and Technology, 47(4), 423-428.
- [52] Tsai, C. L., Lin, Y. J., Liu, C. J., Horng, L., Shih, Y. T., Wang, M. S., ... & Chang, H. C. (2009). Structural, electrical, optical and magnetic properties of Co0. 2AlxZn0. 8– xO films. Applied surface science, 255(20), 8643-8647.
- [53] Machda, F., Ogawa, T., Okumura, H., & Ishihara, K. N. (2020). Damp-heat durability comparison of Al-doped ZnO transparent electrodes deposited at low temperatures on glass and PI-tape/PC substrates. Ceramics International, 46(10), 16178-16184.
- [54] Ji, P. F., Li, Y., Zhou, F. Q., Song, Y. L., & Huang, H. C. (2020). Fabrication and electroluminescence of sheet-like ZnO/Si light-emitting diodes by radio frequency magnetron sputtering method. Materials Letters, 262, 127028.
- [55] Mahroug, A. (2015). Étude des couches minces d'oxyde de zinc dopé aluminium et cobalt élaborées par la technique sol-gel spin coating: Application à la photodétection et au photocourant [Thèse de doctorat, Université Frères Mentouri-Constantine.
- [56] Dev, S., Kumar, P., Rani, A., Agarwal, A., & Dhar, R. (2020). Development of indium doped ZnO thin films for highly sensitive acetylene (C2H2) gas sensing. Superlattices and Microstructures, 145, 106638.
- [57] Tekin, D., Kiziltas, H., & Ungan, H. (2020). Kinetic evaluation of ZnO/TiO2 thin film photocatalyst in photocatalytic degradation of Orange G. Journal of Molecular Liquids, 306, 112905.

Chapter II: Thin films deposition techniques and characterization methods

This chapter is divided into two main sections. The first section focuses on deposition techniques, with particular emphasis on the primary method spray pyrolysis. The second section covers various characterization methods for thin films, including electrical, optical, morphological, and structural analyses.

II.1. Deposition methods:

Thin film technology has undergone significant development due to advancements in materials science and engineering. Thin films, with thicknesses ranging from nanometers to micrometers, are used in various applications such as electronics, optics, and energy generation. The unique properties of these materials at the nanoscale have enabled the development of devices with enhanced performance [1].

Common deposition techniques include thermal evaporation [2], sputtering [3], chemical vapor deposition (CVD)[4], molecular beam epitaxy (MBE) [5], atomic layer deposition (ALD)[6], chemical bath deposition (CBD) [7], and plasma-enhanced chemical vapor deposition (PECVD)[8]. These techniques vary in their advantages and challenges, making them suitable for specific applications and materials [1]. Thin films of zinc oxide can be prepared using various physical or chemical deposition techniques, such as chemical vapor deposition, laser ablation, aerosol spraying or pyrolysis, the sol-gel process, cathodic sputtering, and others [9], as shown in the figure.

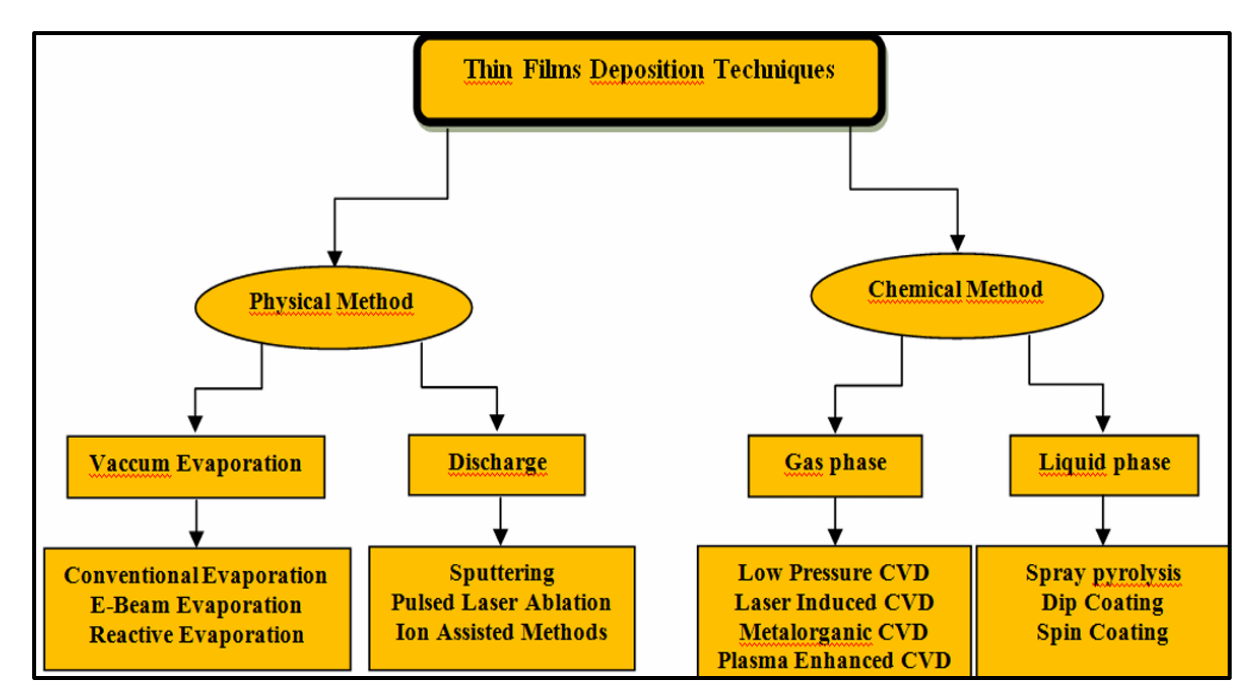


Figure II-1:Classification of different thin film deposition methods. [10]

II.2. Criteria for selection of a deposition technique

The quality and application of the thin films determine the deposition process used. The initial step is to determine which process can synthesize the material to be placed. Factors influencing technique selection include [11]:

- ✓ Type of substance to be deposited.
- ✓ Determine the appropriate deposition rate and layer thickness.
- ✓ The substrate-imposed restrictions.
- ✓ Optimal stoichiometry.
- ✓ Adhesion of deposit to substrate.
- ✓ Reproducibility and cost.

II.3. Choosing the ZnO Deposition Process

Spray pyrolysis is one of the most commonly used techniques for preparing thin films, due to its speed, simplicity in implementation, and suitability for producing large surfaces with an average uniformity. This technique is also used to prepare thick layers. In the context of our work, this method was chosen for the following reasons [12]

II.3.1. Spray pyrolysis

Spray pyrolysis has been used to deposit various types of thin films, which have been applied in numerous devices. Studies have shown that the properties of these deposited films are significantly influenced by the preparation conditions. Spray pyrolysis is a processing technique being explored in research to prepare thin and thick films, ceramic coatings, and powders. This technique is simple and cost-effective compared to many other film deposition methods. It offers an easy way to prepare films with different chemical compositions without requiring high-quality substrates or chemicals. It has been used for several decades in the glass industry and in solar cell production [13]. It has several types, among which we mention: Ultrasonic Spray Pyrolysis (USP) [14], The pneumatic method (PS), Electrostatic Spray Pyrolysis (ESP) [15], Pulsed Spray Pyrolysis (PSP) [16], Aerosol-Assisted Spray Pyrolysis (AASP) [17].

In this work, we employed the **pneumatic pyrolysis spray** (**PSP**) **technique**, which relies on a moderately pressurized air stream to transport a solution containing the desired precursors. Atomization occurs at the nozzle outlet, where the air flow breaks the liquid into fine droplets. These droplets are directed onto a heated substrate, allowing the solvent to evaporate rapidly while the precursors under go thermal decomposition, leading to the formation of a uniform thin film. This method offers good control over film thickness and composition, and is particularly effective for depositing metal oxide layers on various types of substrates.

II.3.1.1. Definition of spray pyrolysis

The "spray pyrolysis" method is a suitable technique for preparing thin films. The term "spray" in English refers to the release of a liquid (such as perfume, deodorant, or insecticide) in the form of a fine mist of droplets. "Pyrolysis," on the other hand, is derived from the word "pyrolytic," which refers to heating the substrate. In this process, thermal decomposition of the source occurs in order to release a metal or a chemical compound. The temperature of the substrate provides the necessary energy, known as activation energy, to initiate the chemical reaction between the compounds [18].

II.3.1.2. Principle

A solution containing the various components of the material to be deposited is sprayed in fine droplets, either using a conventional pneumatic system or an atomizer with an ultrasonic generator. These systems convert the solution into a fine mist of droplets, each with a diameter of a few tens of micrometers (µm). The mist is directed onto the surface of substrates that are heated to a temperature sufficient to decompose the dissolved precursor products in the solution and initiate the reactions that will produce the desired material. At these temperatures, some by-products of the reactions (volatile elements) are immediately eliminated, leaving only the compound to be deposited on the substrate. The process of film formation by the pyrolytic spraying method, known as "Spray Pyrolysis," can be summarized as follows:

- Formation of droplets at the nozzle.
- Decomposition of the precursor solution on the heated substrate surface through pyrolysis reactions [19].

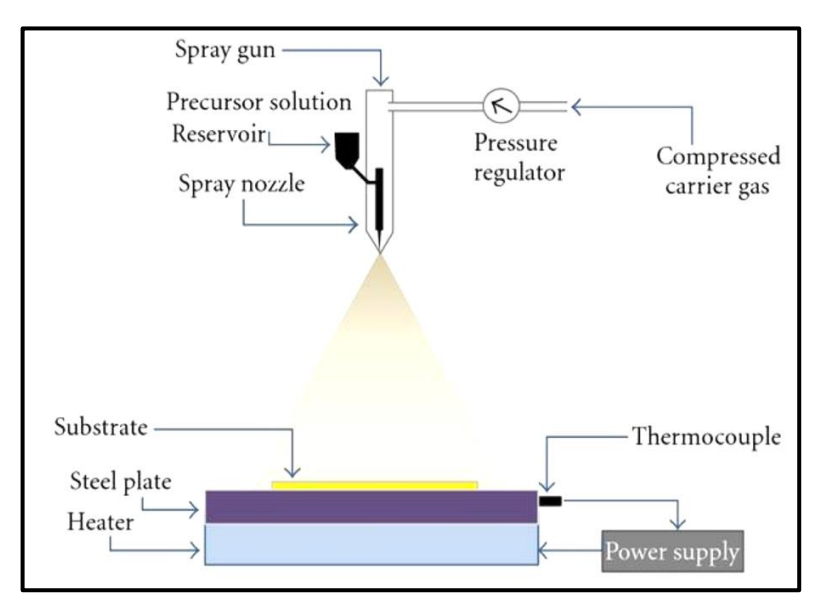


Figure II-2:Spray pyrolysis techniques [20]

II.3.1.3. Model for film deposition by spray pyrolysis:

Thin-film deposition using spray pyrolysis involves three main steps: atomization of the precursor solution, transportation of the resulting aerosol, and decomposition of the precursor on the substrate. There are many complex processes occurring during this process, such as

droplet evaporation, spreading on the substrate, drying, and decomposition, making it difficult to model them directly. Understanding these processes will help improve film quality.

✓ Atomization of precursor solution

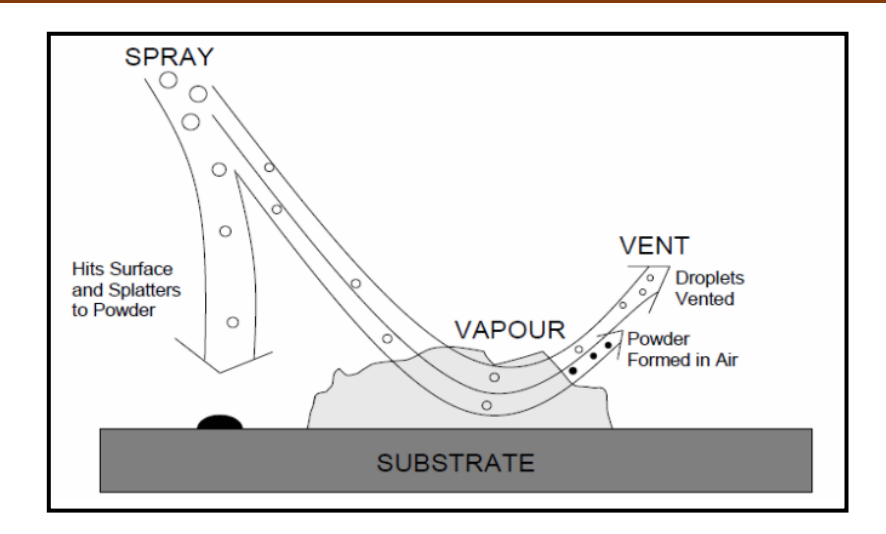
The atomization of liquids is essential in spray pyrolysis techniques, using air blast, ultrasonic, and electrostatic atomizers. The effect of liquid properties on these processes has been studied, with emerging techniques like electrostatic atomization offering precise control over droplet size distribution. Important modes in this process include the "cone-jet" mode, where the liquid is distorted into a conical shape, and the "multi-jet" mode, which occurs when the applied voltage increases, leading to more jets being formed

✓ Aerosol transport

The transport of droplets and solvent evaporation during the spray pyrolysis process have been studied, where droplets are transported to the substrate without forming powder or salt particles. Several forces, such as gravitational, electric, thermophoretic, and temperature gradients, influence the trajectory and evaporation of the droplets. The formation of a porous crust or hollow particles occurs due to rapid solvent evaporation and slow solute diffusion. Studies show that smaller droplets produce solid particles due to faster solute diffusion inside the droplet, while larger droplets lead to the formation of undesirable hollow particles. Additionally, increasing the number of droplets reduces the likelihood of hollow particle formation and impacts the evaporation and precipitation rates.

✓ Decomposition of precursor

During decomposition of the precursor, several operations take place simultaneously (evaporation of residual solvent, spreading of the droplet, and salt decomposition). Substrate temperature and droplet size significantly affect the quality of the deposited film [21] They are identified in Figure (II-3).



FigureII-3: Schematic of aerosol transport by Sears et al. [10]

II.4. Characterization Methods:

After producing thin films, it is critical to perform a number of characterization tests. These tests contribute to the investigation and optimization of parameters such as deposition temperature, doping concentration, and flow rate. These layers will be subjected to a variety of characterization approaches in order to better understand their properties and performance. The methods used to characterize thin films are as follows:

II.4.1. Thickness Measurements

Four techniques can be used to measure the thickness of deposited films: the Scanning Electron Microscope (SEM), which provides high precision for thick films but struggles to measure thin films, profilometry, which is used to measure thickness easily and accurately without the need for complex sample preparation, and spectrophotometry, which relies on interference in the transmission spectrum to determine thickness [22]. Additionally, there is another method for measuring the thickness of films using the mass difference method, where the thickness is determined based on light absorption in the spectrophotometer, taking into account the surface area and the density of the studied thin film. Due to the limitations of SEM and spectrophotometry in certain cases, profilometry is considered the optimal choice for measuring the thickness of thin films [23].

$$t = \frac{\Delta m}{s\rho} \tag{II.1}$$

Where: S and ρ are respectively the surface area and the density of the studied thin film.

II.4.2. Structural Characterization:

II.4.2.1.X-Ray Diffraction:

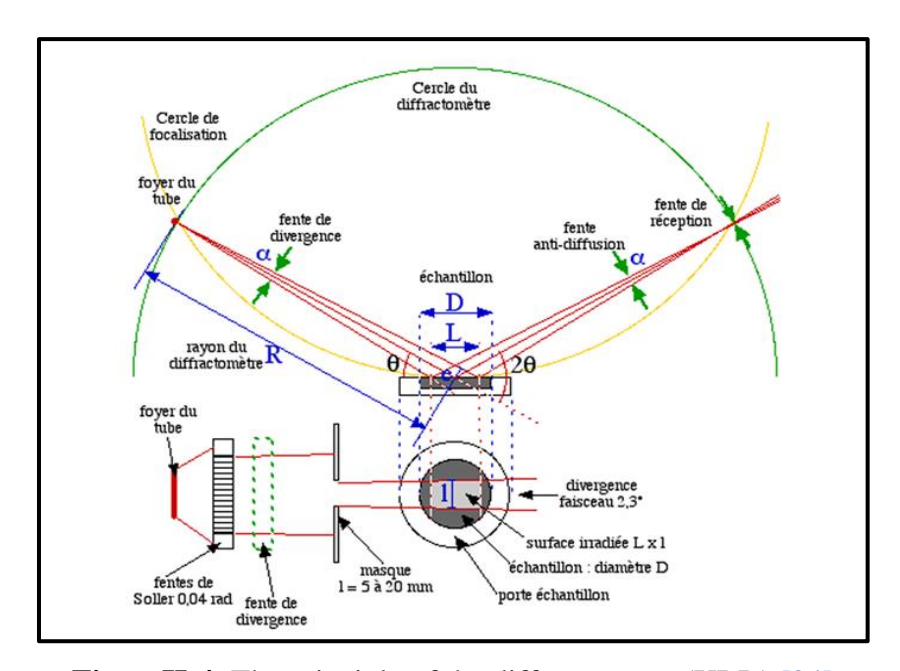
X-ray diffraction (XRD) is a widely used technique for investigating the structural properties of materials. X-rays, with wavelengths between 0.1 and 10 Å, belong to the electromagnetic spectrum and are well-suited for probing atomic-scale structures. They exhibit dual characteristics: wave-like and particle-like. In the particle-like case, X-rays can be considered as a group of particles traveling at the speed of light, and their energy is given by the equation [24]:

$$E = h\nu = \frac{hc}{\lambda} \tag{II.2}$$

where **h** is Planck's constant.

X-ray diffraction allows for determining the structure, crystalline phase, lattice parameters, crystallite size, and the stresses exerted on the layer during deposition. The principle of this technique is based on Bragg's equation [25,26]:

$$2d_{hkl}\sin\theta = n\lambda \tag{II.3}$$



FigureII-4: The principle of the diffractometer (XRD) [24]

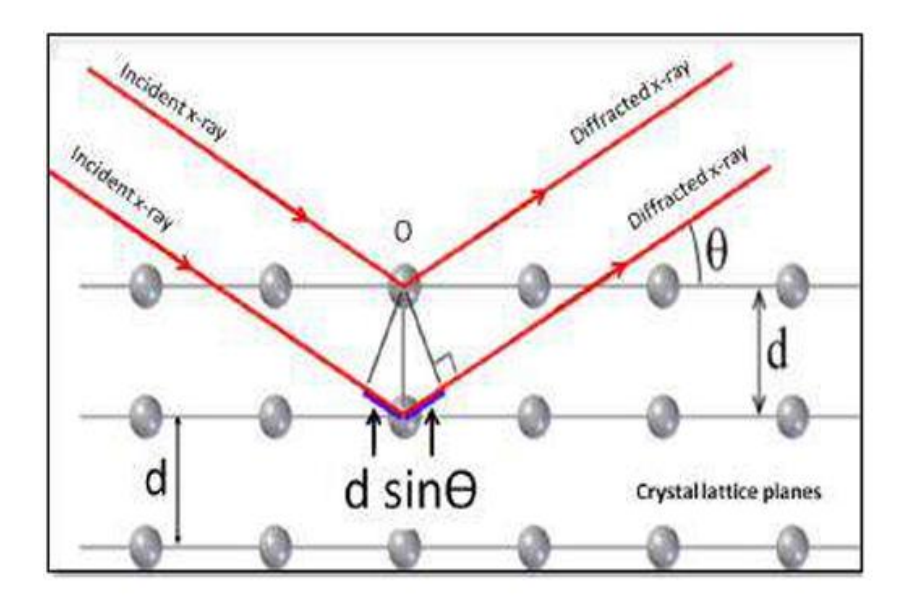


Figure II-5: X-Ray Diffraction [27]

where d_{hkl} is the interplanar distance between planes defined by the Miller indices (h, k, l), θ is the angle of incidence of the X-rays on the surface of the material under study, n is the diffraction order, and λ is the wavelength of the X-ray beam. By combining Bragg's law, which relates the interplanar distance of a crystal to the Miller indices, it is possible to determine the angles at which the (hkl) planes diffract, based on a Lattice parameters refer to the dimensions of a unit cell. In the case of the hexagonal wurtzite structure, as in our study of ZnO, we focus on two main parameters: the distance between two adjacent zinc atoms in a horizontal plane α and the largest distance between two zinc atoms in two adjacent planes c.

The interplanar distance d_{hkl} is related to the lattice parameters as well as the Miller indices by the following relation [28,29]:

$$\frac{1}{d_{hkl}^2} = \frac{3}{4} \left(\frac{h^2 + hk + k^2}{a^2} \right) + \frac{l^2}{c^2}$$
 (II.4)

 d_{hkl} : Interreticular distance.

c, a: Crystal parameters.

(hkl): Miller indices.

The lattice parameters (a=b, c) have been calculated using the following equation [30,31]:

$$a = \frac{\lambda}{\sqrt{3}\sin\theta_{(100)}} \tag{II.5}$$

$$c = \frac{\lambda}{\sin \theta_{(002)}} \tag{II.6}$$

II.4.2.2. Measurement of Grain Size, dislocation density and strain:

Among the main applications of X-ray diffraction, this technique is used to calculate the grain size of different samples. To ensure accurate grain size values for our films, we used the Scherrer equation [32,33].

$$D = \frac{0.94\lambda}{\beta \cos \theta} \tag{II.7}$$

Where:

- **D** is the grain size (in nanometers).
- λ is the wavelength of the X-ray beam ($\lambda = 0.154183$ nm).
- θ is the diffraction angle (in radians).
- β is the full width at half maximum (in radians).

The dislocation density (δ) in the thin film can also be calculated using the grain size (D) with the following relation [34]:

$$\delta = \frac{1}{n^2} \tag{II.8}$$

The strain induced in the film was calculated using the relation [10,35]

$$\varepsilon = \frac{\beta \cos \theta}{4} \tag{II.9}$$

II.4.2.3. Determination of Stresses

Stresses are internal forces within the material. The relationship that links stresses $(\sigma_{ij}[Pa])$, straintensors (ε_{kl}) , and elastic constants (C_{ijkl}) is given by the following equation:

$$\sigma_{ij} = C_{ijkl} \cdot \varepsilon_{kl} \tag{II.10}$$

The internal stresses of ZnO can be calculated using the following equations [36,37]

$$\sigma = -238,2 \left(\frac{c - c_0}{c_0}\right) \tag{II.11}$$

where $c_0 = 5.2066 \text{Å}$ is the bulk standard lattice constant of ZnO along the c-axis according to the JCPDS: 36-1451 and c is lattice parameter of thin films deposited.

These stresses affect the crystal structure by causing either compressive or tensile displacement as shown in the figure II-6.

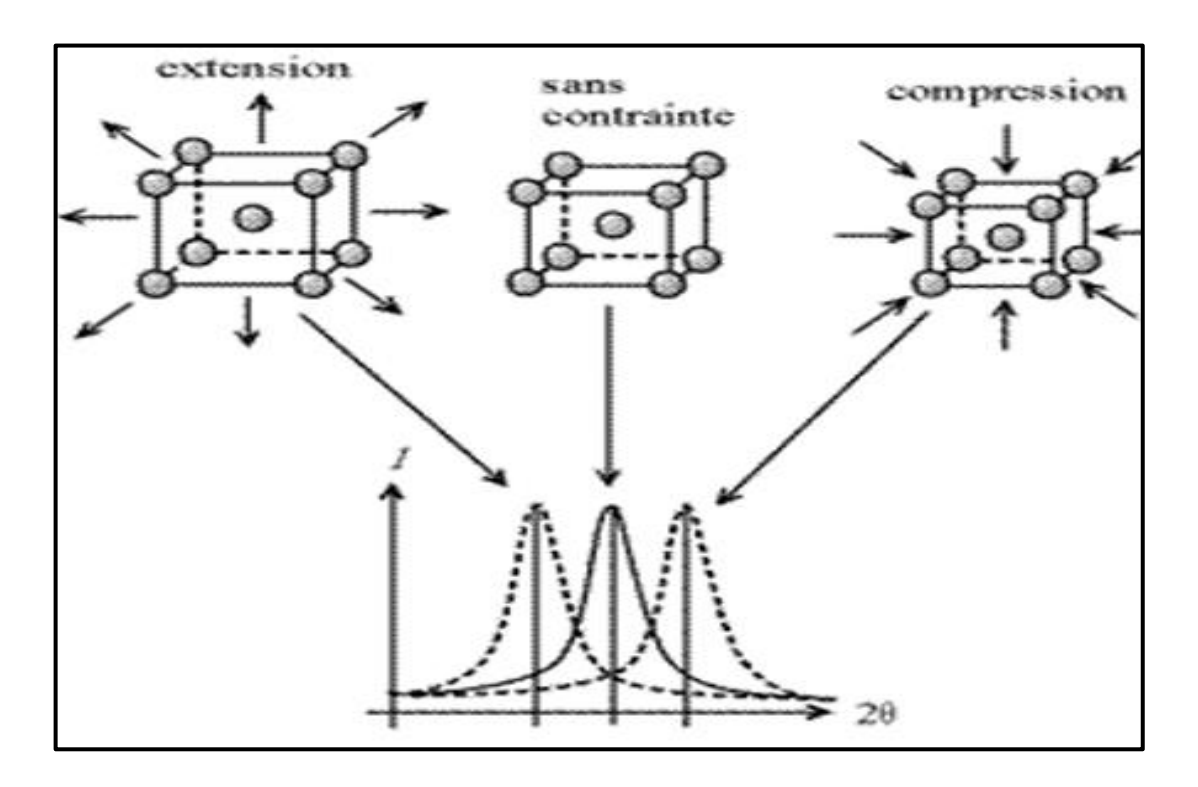


Figure II-6: Peak Shift and Strain Type in XRD Pattern [38]

II.4.3. Optical Characterization

II.4.3.1. UV-visible spectroscopy

UV-Visible spectroscopy is a non-destructive optical characterization technique that allows working with small quantities of substances. It is used in a wide range of analytical applications, providing information about the optical properties of the sample, such as light transmission and absorption, estimation of the optical gap, and crystallite sizes. In some cases, it can also provide information about the sample's thickness and even its optical constants.

The principle of this technique is based on the interaction of emitted light with the sample being analyzed. Part of the incident beam is absorbed or transmitted by the sample. When a substance absorbs light in the ultraviolet and visible range, the absorbed energy causes disturbances in the electronic structure of the atoms, ions, or molecules. One or more electrons absorb this energy and jump from a lower energy level to a higher energy level. These electronic transitions occur in the visible range between 350 and 800 nm, and in the ultraviolet range between 200 and 350 nm.[39]

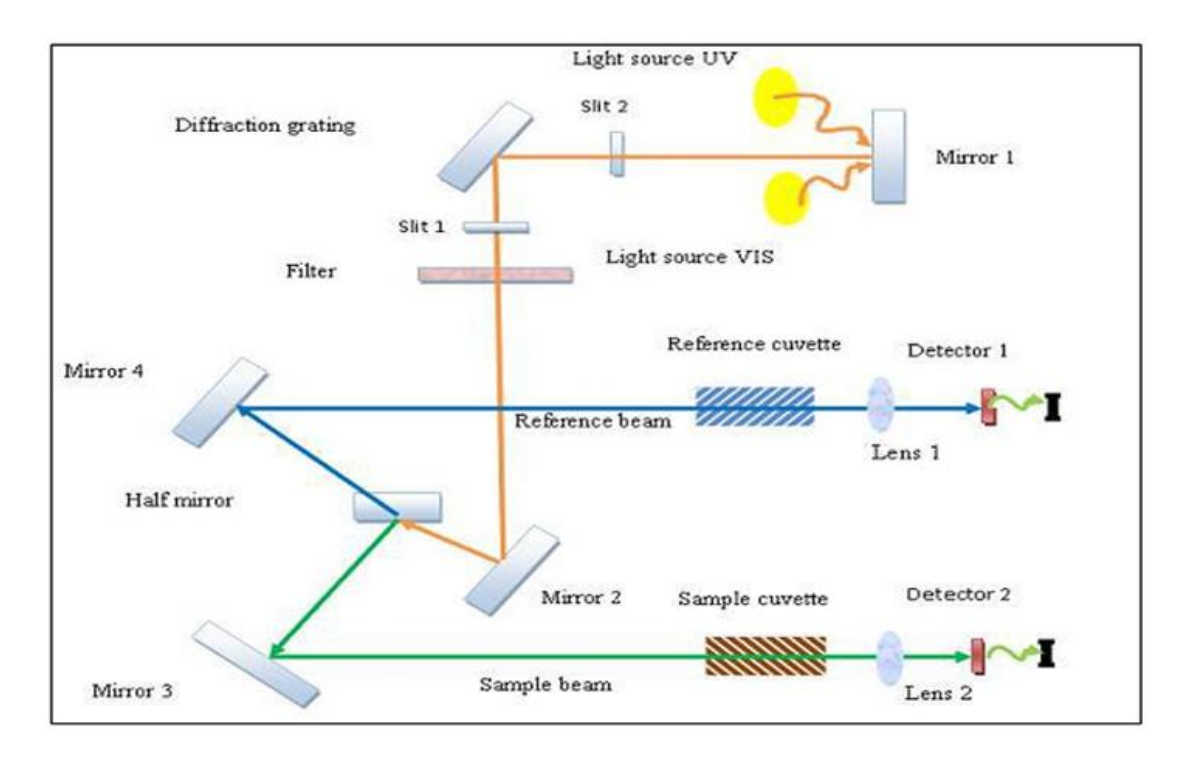


Figure II-7: Schematic representation of the UV-Visible spectrophotometer [40]

II.4.3.2. Optical Band Gap

By analyzing the transmission spectrum of a given layer, the absorption coefficient α alpha α of the material constituting the layer can be calculated using the Bouguer-Lambert-Beer relation, commonly known as Beer's law [41]:

$$T = T_0 e^{-\alpha t} \tag{II.12}$$

If the transmittance T is expressed as a percentage, the absorption coefficient is given by the following formula [42,43]:

$$\alpha = \frac{1}{t} \ln \left(\frac{100}{T(\%)} \right)$$
 and $\alpha = \frac{4k}{\pi \lambda}$ (II. 13)

Where:

- t is the thickness of thin films.
- T is the transmittance.
- k is the extinction coefficient.
- λ is the wavelength of light.

the determination of the optical gap is based on the model proposed by Tauc, where E_g is related to the absorption coefficient α by the following equation: [44,45]

$$(\alpha h \nu)^2 = A(h\nu - E_a) \tag{II.14}$$

Where: hv is the photon energy, Eg is optical gap n and A are constants, n characterizes the optical type of transition and takes the values 2, 1/2 (2 for allowed direct transitions or $\frac{1}{2}$ for allowed indirect transitions).

Thus, by plotting $(\alpha h v)^2$ as a function of photon energy (h v), and by extrapolating the linear portion of the $(\alpha h v)^2$ curve to intersect the x-axis (i.e., where $(\alpha h v)^2 = 0$), we can determine the value of Eg.

$$h\nu(eV) = \frac{h\nu}{\lambda} = \frac{1240}{\lambda(\text{Å})}$$
 (II. 15)

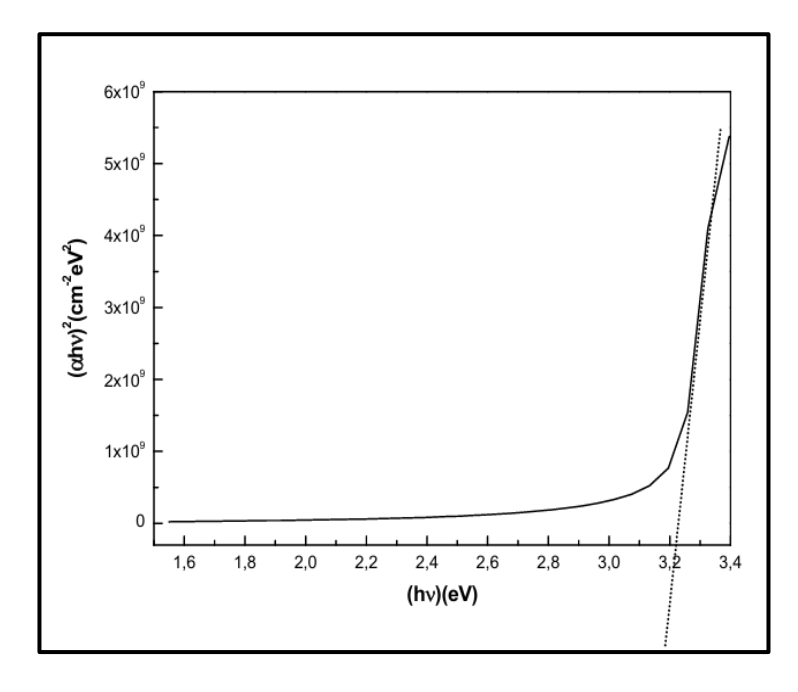


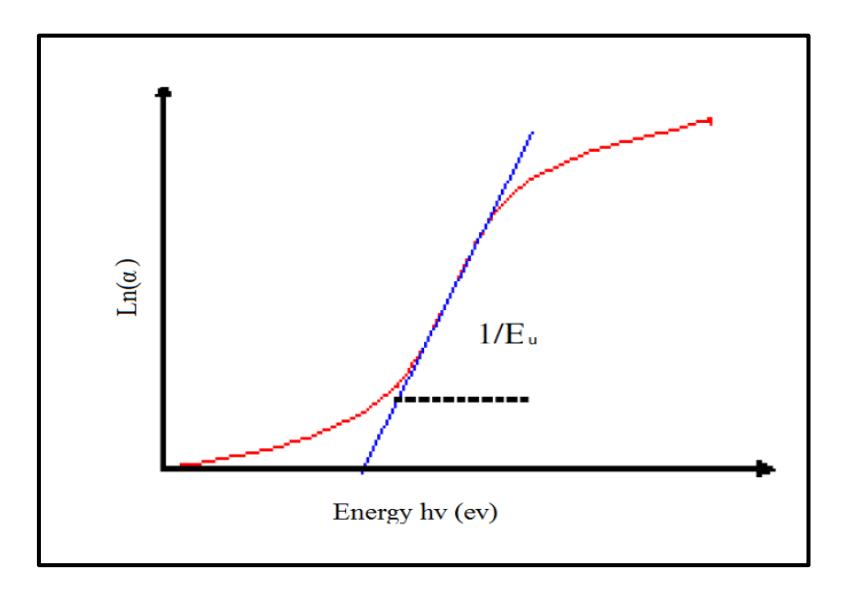
Figure II-8: determination of the gap [46]

II.4.3.3. Urbach Energy

In general, during optical absorption near the band edges, electrons are excited from the top of the valence band to the bottom of the conduction band across the energy band gap. During this transition process, if these electrons experience disorder, it leads to the tailing of the density of states $\rho(h\nu)$, where $h\nu$ is the photon energy, into the energy gap. This tail extending into the gap energy is called the Urbach tail. As a result, the absorption coefficient $\alpha(h\nu)$ also decays exponentially, and the energy associated with this decay is referred to as the Urbach energy, which can be calculated using the following equation

$$\alpha(h\nu) = \alpha_0 ex \, p\left(\frac{h\nu}{E_u}\right) \tag{II.16}$$

Where α_0 is a constant, hv is the photon energy, and Eu is the Urbach energy. The Urbach energy is determined by plotting $\ln(\alpha)$ versus hv and fitting the linear portion of the curve with a straight line. The reciprocal of the slope of the linear region gives the Eu value. The Eu values of the samples decrease in the case of crystallization at higher temperatures. This is because the Urbach energy in glassy semiconductors fundamentally defines the level of disorder, and crystallization and the resulting order from this process reduce the Eu value. [47]



FigureII-9 Urbach energy determination [48]

II.4.3.4. Refractive index

The correlation between the refractive index and the energy band gap in semiconductors has attracted significant research interest over the past decades. This line of study began with the semi-empirical relation proposed by Moss in 1950. Since then, numerous similar relations have been introduced to estimate the refractive index of materials. In this section, we review and analyze the most prominent of these relations as reported in the scientific literature, as they are widely used to calculate the refractive index based on the energy band gap [49,50].

Ravindra relation:
$$n = 4.048 - 0.62E_g \tag{II.17}$$

Herve–Vandamme relation:
$$n^2 = 1 + \left[\frac{A}{B + E_g}\right]^2$$
 (II. 18)

Where A and B are experimental constants with values A = 13.6 eV and B = 3.4 eV

II.4.4. Morphological Characterization of Thin Films

II.4.4.1. Scanning Electron Microscope (SEM)

The Scanning Electron Microscope (SEM) uses electrons to produce high-resolution images with a large depth of field, allowing detailed observation of conductive samples. Its ease of sample preparation and exceptional magnification and focus make it essential in modern research and development.

The electron flow passes through a condenser lens and is focused onto a very small point on the sample by the objective lens. When the electron beam strikes the sample, secondary electrons are produced and collected by a secondary detector or backscattered electron detector, then converted into a voltage and amplified. This amplified voltage is applied to the Cathode Ray Tube (CRT) screen, where it alters the intensity of the light spot, creating an image made up of varying light spots corresponding to the sample's topography.

SEM must always be used in a vacuum to prevent sample contamination or ionization of background gases, which can affect the measurements [51].

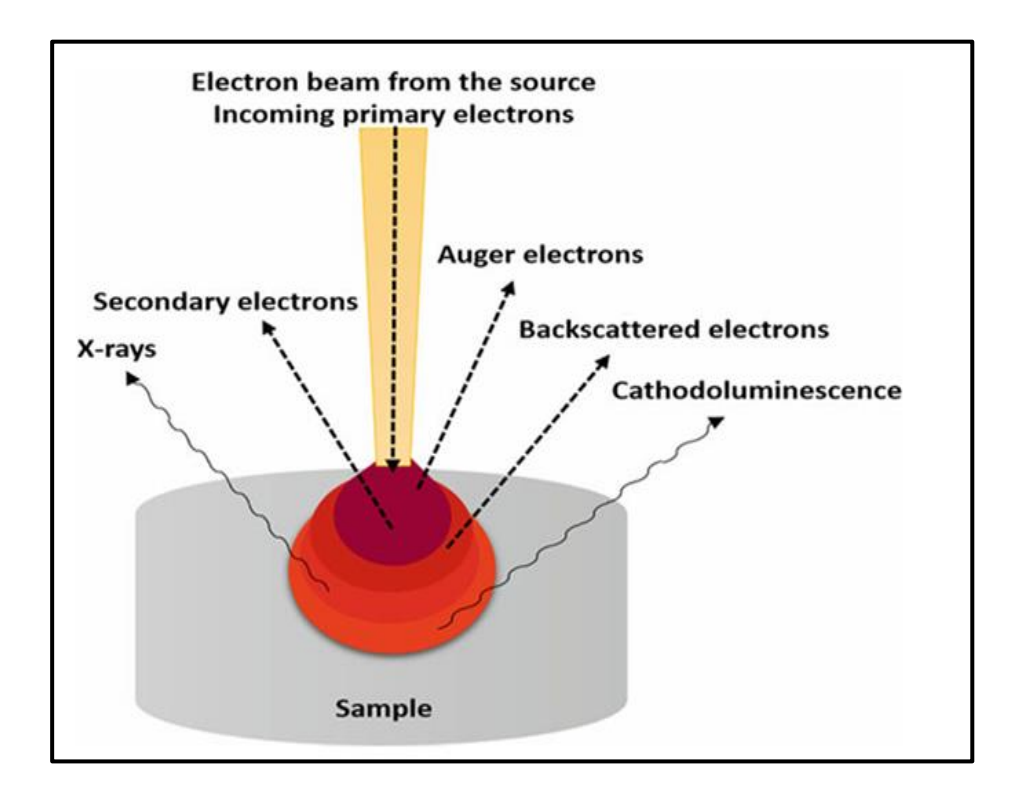


Figure II-10: The interaction of electron beam with specimen and the signal emitted from the sample [52]

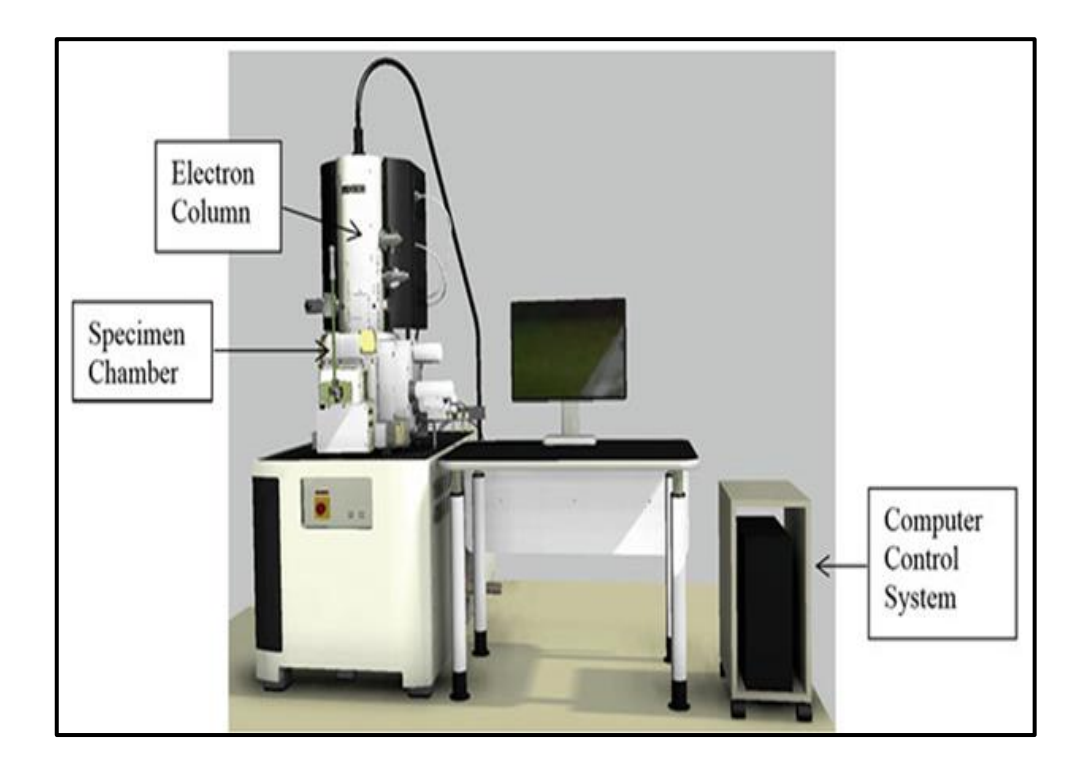
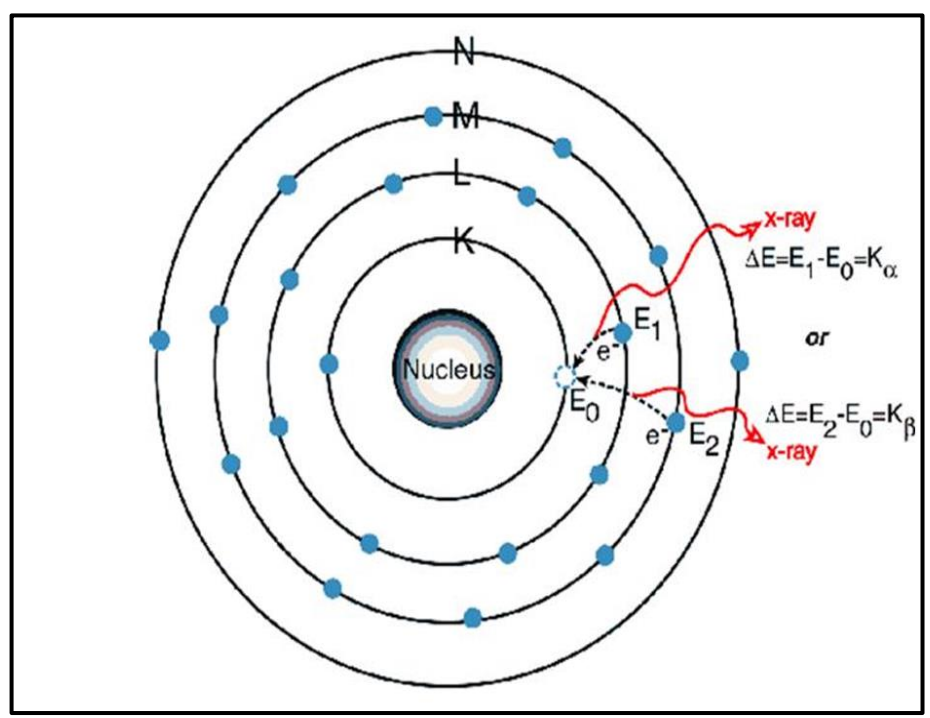


Figure II-11: A photograph showing three major sections of the SEM: the electron column, the specimen chamber, and the computer control system [53]

II.4.4.2. Energy dispersive X-ray spectroscopy (EDS or EDX)

EDX (Energy Dispersive X-ray) spectroscopy is used to detect the elemental composition of a substance using a Scanning Electron Microscope (SEM). It can detect elements with atomic numbers higher than boron at concentrations as low as 0.1%. The technique works by stimulating the sample with an electron beam, which results in the emission of characteristic X-rays that can be used to identify the elements and measure their concentrations. The emitted X-rays are divided into two types: X-ray continuum (generated by the deceleration of electrons) and characteristic X-rays (produced when an electron from an outer shell fills the inner shell vacancy). EDX is used in applications such as material evaluation, contamination detection, spot analysis, and quality control screening.[54] When a high-energy electron strikes the sample, it may eject an electron from the inner shell of an atom, leaving behind a vacancy. Electrons from higher energy levels then drop down to fill this vacancy in the inner shell, and during this transition, a photon is emitted with an energy equal to the difference between the two energy levels (FigureII.12). The emitted photon typically falls within the X-ray frequency range of the electromagnetic spectrum [55]



FigureII-12: Scheme of X-ray excitations in EDX analysis [55]

II.4.4.3. Fourier Transform Infrared Spectroscopy (FTIR)

Infrared spectroscopy is a powerful technique for identifying materials by analyzing their absorption or reflection of electromagnetic radiation. It reveals structural information, especially the nature of cation—oxygen bonds, as vibrational frequencies depend on cation mass, bond type, and lattice parameters. The spectra provide both qualitative data identifying chemical groups based on absorbed wavelengths and quantitative data estimating their concentrations through absorption intensity.

This technique is effective for analyzing almost all types of samples, regardless of their physical state or surface condition. The measurement principle involves detecting the amount of light absorbed as a function of wavelength during the interaction between radiation and matter, typically within the 4000–400 cm⁻¹ range. Absorption occurs when the radiation frequency matches a vibrational frequency of molecules or atomic groups, and this frequency depends on the bond nature, atomic masses, and the surrounding environment. Spectra are commonly obtained using interferometers and processed through Fourier Transform Infrared Spectroscopy (FTIR) [56].

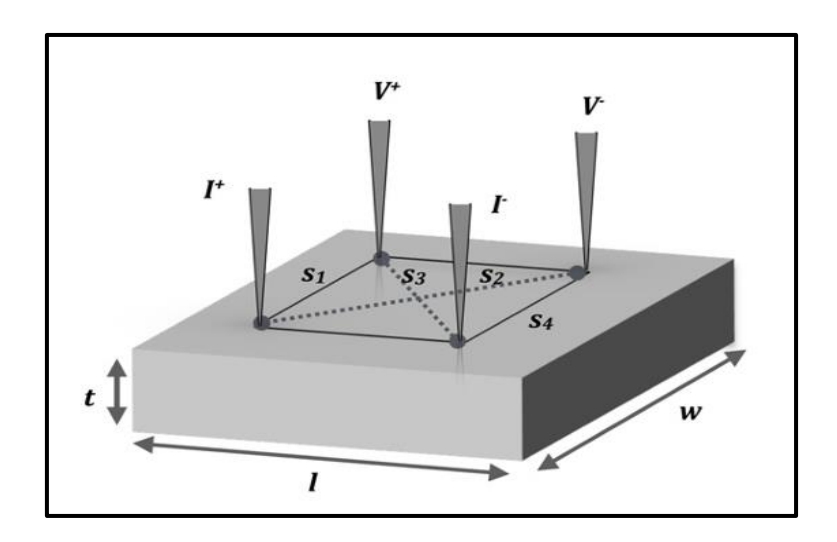


FigureII-13: infrared spectrometer [56]

II.4.5. Electrical Characterization

II.4.5.1. Four-point-probe Method

The four-point probe technique is designed to measure the resistivity of semiconductor materials, whether in bulk form or as thin films, with different formulas applied depending on the sample type. The method is based on a simple principle: an electric current is applied through the outer probes, while the voltage is measured between the inner probes. This setup allows for accurate determination of the sample's resistivity. A schematic diagram of the setup is shown below. Figure (II-14) illustrates the four-point probe measurement setup, where a current (I) is passed through the sample and the voltage (V) is measured as shown. The specific resistivity (ρ) of the sample can then be calculated [57].



FigureII-14: Schematic of a square 4Pprobe configuration [58]

II.4.5.2. Electrical Resistivity Measurement

Unlike a bulk sample, measuring the electrical properties of this thick sheet requires that the sample thickness the less than the distance between the probes. This is because the electric current overlaps at the ends of the outer probes, leading to a modified resistance calculation, which is given by [59]:

$$R_s = \frac{\pi V}{\ln 2 I} \tag{II.19}$$

The **resistivity** ρ can be calculated using the following equation:

$$\rho = \left(\frac{\pi t}{\ln^2 t}\right) \cdot t = R_s \cdot t \tag{II.20}$$

The **electrical conductivity** $\boldsymbol{\sigma}$ is then the reciprocal of the resistivity:

$$\sigma = \frac{1}{\rho} \tag{II.21}$$

References

- [1] Toma, F. T. Z., Rahman, M. S., Hussain, K. M. A., & Ahmed, S. (2024). Thin film deposition techniques: A comprehensive review. Journal of Modern Nanotechnology, 4(1), Article 2788-8118.
- [2] Vishwakarma, R. (2015). Effect of substrate temperature on ZnS films prepared by thermal evaporation technique. Journal of Theoretical and Applied Physics, 9, 185-192.
- [3] Berg, S., & Nyberg, T. (2005). Fundamental understanding and modeling of reactive sputtering processes. Thin solid films, 476(2), 215-230.
- [4] Frey, H. (2015). Chemical vapor deposition (CVD). In Handbook of Thin-Film Technology (pp. 225-252). Berlin, Heidelberg: Springer Berlin Heidelberg.
- [5] Arthur, J. R. (2002). Molecular beam epitaxy. Surface Science, 500(1-3), 189–217.
- [6] Leskelä, M., & Ritala, M. (2002). Atomic layer deposition (ALD): from precursors to thin film structures. Thin solid films, 409(1), 138-146.
- [7] Gujar, T. P., Shinde, V. R., Lokhande, C. D., Mane, R. S., & Han, S. H. (2005). Bismuth oxide thin films prepared by chemical bath deposition (CBD) method: annealing effect. Applied surface science, 250(1-4), 161-167.
- [8] Martinu, L., Zabeida, O., & Klemberg-Sapieha, J. E. (2010). Plasma-Enhanced Chemical Vapor Deposition of functional coatings. In P. M. Martin (Ed.), Handbook of Deposition Technologies for Films and Coatings (pp. 392–465). Elsevie.
- [9] Lameche, N. E. H. (2017). Effet du laser et du milieu environnant de dépôt sur les performances des films des oxydes transparents [Thèse de doctorat de 3° cycle, Université Ferhat Abbas Sétif 1]
- [10] Bennaceur, K. (2020). Elaboration and characterization of SnO2: In thin films deposited by spray pyrolysis technique (Doctoral dissertation, University Mohamed Khider Biskra).
- [11] Baghriche, L. (2015). Élaboration et caractérisation des couches minces d'oxyde de zinc et sulfure de zinc préparées par spray ultrasonique [Thèse de doctorat, Université Frères Mentouri].

- [12] SALIM, K. (2020). Amélioration des propriétés électriques et optiques des couches minces de ZnO destinées aux applications photovoltaïques [Thèse de doctorat, Université Djillali Liabes de Sidi Bel Abbès]
- [13] Bouaichi, F. (2019). Deposition and analysis of Zinc Oxide thin films elaborated using spray pyrolysis for photovoltaic applications (Doctoral dissertation, University Mohamed Khider of Biskra).
- [14] Majerič, P., & Rudolf, R. (2020). Advances in ultrasonic spray pyrolysis processing of noble metal nanoparticles. Materials, 13(16), 3485.
- [15] Zaouk, D., Zaatar, Y., Asmar, R., & Jabbour, J. (2006). Piezoelectric zinc oxide by electrostatic spray pyrolysis. *Microelectronics journal*, *37*(11), 1276-1279.
- [16] Subramanian, M., Thakur, P., Tanemura, M., Hihara, T., Ganesan, V., Soga, T., Chae, K. H., Jayavel, R., & Jimbo, T. (2010). Intrinsic ferromagnetism and magnetic anisotropy in Gd-doped ZnO thin films synthesized by pulsed spray pyrolysis method. Journal of Applied Physics, 108(5), 053912
- [17] Nie, P., Xu, G., Jiang, J., Dou, H., Wu, Y., Zhang, Y., ... & Zhang, X. (2018). Aerosol-spray pyrolysis toward preparation of nanostructured materials for batteries and supercapacitors. Small Methods, 2(2), 1700272.
- [18] Haffas, S., & Berak, M. (2020). Caractérisation des couches minces Co₃O₄:Cu élaborées par la technique spray pneumatique [Mémoire de master, Université Mohamed Khider de Biskra]
- [19] Taabouche, A. (2015). Etude structurale et optique de films minces ZnO élaborés par voie physique et/ou chimique (Doctoral dissertation, Université de Constantine 1).
- [20] Janarthanan, B., Thirunavukkarasu, C., Maruthamuthu, S., Manthrammel, M. A., Shkir, M., AlFaify, S., ... & Park, C. (2021). Basic deposition methods of thin films. Journal of Molecular Structure, 1241, 130606.
- [21] Perednis, D., & Gauckler, L. J. (2005). Thin film deposition using spray pyrolysis. Journal of electroceramics, 14, 103-111.

- [22] Rahmane, S. (2008). LABORATION ET CARACTERISATION DE COUCHES MINCES PAR SPRAY PYROLYSE ET PULVERISATION MAGNETRON (Doctoral dissertation, Université Mohamed Khider Biskra).
- [23] Benkhetta, O. (2019). Effet de la concentration de la solution sur les propriétés des couches minces de dioxyde de titane déposées par spray pyrolyse ultrasonique [Mémoire de master, Université Mohamed Khider de Biskra].
- [24] Slimi, H. (2019). Élaboration et caractérisation de couches minces co-dopées In, Co, préparées par la pulvérisation cathodique, applications aux cellules photovoltaïques (Doctoral dissertation, Université du Littoral Côte d'Opale; Université de Sfax. Faculté des sciences).
- [25] Banarescu, A., & Baltag, O. (2006). The Bragg diffraction modeling using ultrasounds. Condensed Matter, Faculty of Biomedical Engineering, University of Medicine and Pharmacy "Gr. T. Popa"–Iași. Received September 26, 2006.
- [26] Ladd, M. F. C. (1972). X-ray reflection and the Bragg equation. Physics Education, 7(6), 368.
- [27] Bourfa, F., & Attaf, N. (2020). Deposition of ZnO thin films for treatment of water (Doctoral dissertation, Université Frères Mentouri-Constantine 1).
- [28] Al-Ghamdi, A. A., Al-Hartomy, O. A., El Okr, M., Nawar, A. M., El-Gazzar, S., El-Tantawy, F., & Yakuphanoglu, F. (2014). Semiconducting properties of Al doped ZnO thin films. Spectrochimica Acta Part A: Molecular and Biomolecular Spectroscopy, 131, 512-517.
- [29] Devesa, S., Rooney, A. P., Graça, M. P., Cooper, D., & Costa, L. C. (2021). Williamson-hall analysis in estimation of crystallite size and lattice strain in Bi1. 34Fe0. 66Nb1. 34O6. 35 prepared by the sol-gel method. Materials Science and Engineering: B, 263, 114830.
- [30] Kumar, V., Kumar, V., Som, S., Yousif, A., Singh, N., Ntwaeaborwa, O. M., ... & Swart, H. C. (2014). Effect of annealing on the structural, morphological and photoluminescence properties of ZnO thin films prepared by spin coating. Journal of colloid and interface science, 428, 8-15.
- [31] Lupan, O., Pauporté, T., Chow, L., Viana, B., Pellé, F., Ono, L. K., ... & Heinrich, H. (2010). Effects of annealing on properties of ZnO thin films prepared by electrochemical deposition in chloride medium. *Applied Surface Science*, 256(6), 1895-1907.

- [32] LEHRAKI, N. (2021). Dépôt et Caractérisation des couches minces de ZnO par spray ultrasonique (Doctoral dissertation, Université de mohamed kheider biskra).
- [33] Popova, A. N. (2017). Crystallographic analysis of graphite by X-Ray diffraction. Coke and Chemistry, 60, 361-365.
- [34] Yıldırım, M. A., & Ateş, A. (2010). Influence of films thickness and structure on the photo-response of ZnO films. Optics Communications, 283(7), 1370-1377.
- [35] Benamra, H. (2013). L'effet de la température du substrat et de la molarité sur les propriétés des couches minces de sulfure de zinc déposées par spray ultrasonique [Mémoire de magister, Université Mohamed Khider-Biskra]
- [36] Şenadim, E., Kavak, H., & Esen, R. (2006). The effect of annealing on structural and optical properties of ZnO thin films grown bypulsed filtered cathodic vacuum arc deposition. Journal of Physics: Condensed Matter, 18(27), 6391.
- [37] Kahouli, M., Barhoumi, A., Bouzid, A., Al-Hajry, A., & Guermazi, S. (2015). Structural and optical properties of ZnO nanoparticles prepared by direct precipitation method. *Superlattices and Microstructures*, 85, 7-23.
- [38] Hamani, N. (2021). Elaboration et caractérisation des couches minces d'oxyde d'indium dopées à l'étain et au brome obtenue par spray pyrolyse ultrasonique (Doctoral dissertation, Université de mohamed kheider biskra).
- [39] Benelmadjat, H. (2011). Élaboration et caractérisation de matériaux cristallins ou amorphes purs et dopés [Thèse de doctorat en science, Université Mentouri-Constantine].
- [40] Benramache, S. (2012). Elaboration et caractérisation des couches minces de ZnO dopées cobalt et indium (Doctoral dissertation, Université Mohamed Khider-Biskra).
- [41] Khechba, M., & Bouabellou, A. (2018). Elaboration et étude des couches minces d'oxyde d'étain (Doctoral dissertation, Université Frères Mentouri-Constantine 1).
- [42] Bandyopadhyay, S., Paul, G. K., & Sen, S. K. (2002). Study of optical properties of some sol–gel derived films of ZnO. Solar Energy Materials and Solar Cells, 71(1), 103-113.
- [43] Reynolds, D. C., Look, D. C., & Jogai, B. (1997). Optical constants of ZnO. *Japanese Journal of Applied Physics*, 36(10R), 6237–6241

- [44] Chennoufi, A. (2012). L'effet de la molarité et de la température du substrat sur les Propriétés des couches minces d'oxyde d'indium déposées Par spray ultrasonique (Doctoral dissertation Université de mohamed kheider biskra).
- [45] Viezbicke, B. D., Patel, S., Davis, B. E., & Birnie III, D. P. (2015). Evaluation of the Tauc method for optical absorption edge determination: ZnO thin films as a model system. physica status solidi (b), 252(8), 1700-1710.
- [46] Bouhssira, N. (2013). Élaboration des films minces d'oxyde de zinc par évaporation et par pulvérisation magnétron et étude de leurs propriétés [Thèse de doctorat en sciences, Université Constantine 1].
- [47] Benhamida, S. (2018). Caractérisation des couches minces d'oxyde de nickel (NiO) élaboré par spray pyrolyse [Thèse de doctorat en sciences, Université d'Ouargla].
- [48] BEGGAS, A. (2018). Elaboration and characterization of chalcogenide thin films by chemical bath deposition technique (Doctoral dissertation, UNIVERSITE Mohamed Khider Biskra).
- [49] Hervé, P., & Vandamme, L. K. J. (1994). General relation between refractive index and energy gap in semiconductors. Infrared physics & technology, 35(4), 609-615.
- [50] Tripathy, S. K. (2015). Refractive indices of semiconductors from energy gaps. Optical materials, 46, 240-246.
- [51] Manoj, R. (2006). Characterisation of transparent conducting thin films grown by pulsed laser deposition and RF magnetron sputtering [Doctoral dissertation, Cochin University of Science and Technology]
- [52] Akhtar, K., Khan, S. A., Khan, S. B., & Asiri, A. M. (2018). Scanning electron microscopy: Principle and applications in nanomaterials characterization (pp. 113-145). Springer International Publishing.
- [53] Ul-Hamid, A. (2018). A beginners' guide to scanning electron microscopy (Vol. 1, pp. 309-359). Cham: Springer International Publishing.

- [54] Abd Mutalib, M., Rahman, M. A., Othman, M. H. D., Ismail, A. F., & Jaafar, J. (2017). Scanning electron microscopy (SEM) and energy-dispersive X-ray (EDX) spectroscopy. In Membrane characterization (pp. 161-179). Elsevier
- [55] Holsgrove, K. (2017). Transmission electron microscopy study of domains in ferroelectrics (Doctoral dissertation, Queen's University Belfast).
- [56] Filali, H. (2022). Élaboration et caractérisation de l'aluminate de zinc nanocristallin (pur et dopé) synthétisé par la méthode sol-gel [Thèse de doctorat en sciences, Université Frères Mentouri Constantine 1]
- [57] Alnes, M. E. (2014). Transparent conducting oxides by atomic layer deposition [Doctoral dissertation, University of Oslo].
- [58] Miccoli, I., Edler, F., Pfnür, H., & Tegenkamp, C. (2015). The 100th anniversary of the four-point probe technique: the role of probe geometries in isotropic and anisotropic systems. Journal of Physics: Condensed Matter, 27(22), 223201.
- [59] Waremra, R. S., & Betaubun, P. (2018). Analysis of electrical properties using the four-point probe method. In E3S Web of conferences (Vol. 73, p. 13019). EDP Sciences.

Chapter III Experimental Results and Discussion

In this chapter, thin films of zinc oxide doped with aluminum, cobalt, and co-doped with both (Al–Co) were prepared using the pneumatic spray pyrolysis technique. The structural, optical, and electrical properties of these films were studied in order to evaluate the effect of the dopant type on the microstructure, optical response, and electrical behavior of the prepared samples.

III.1. Experimental method

III.1.1. Pneumatic spray pyrolysis technique

This work was completed in the Thin Films Laboratory and applications (LPCMA) at the University of Biskra. Pneumatic spray pyrolysis (PSP) is the process used to deposit our thin films. As shown in the figure III-1.

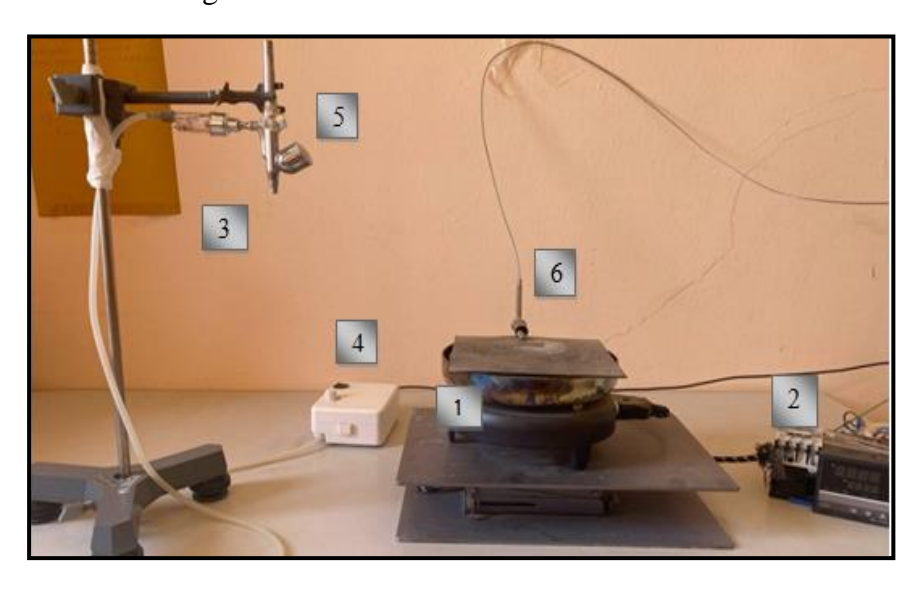


Figure III-1: Spray Pyrolysis Device

Deposition device components:

- 1. include a sample holder and heated plate.
- 2. A temperature regulator is attached to a thermocouple to monitor the temperature.
- 3. Use the atomizer to reduce the solution to fine droplets.
- 4. Air compressor.

- 5. Solution vial.
- 6. Thermocouple.

III.1.2 Preparation of substrates and precursor solutions

III.1.2.1 Preparation of substrates

- a) Choice of the substrate : Glass slides of identical dimensions (L = 25 mm, W = 15 mm
 Characterized by
 - ✓ Its thermal expansion coefficient is similar to that of ZnO ($\alpha = 8.5 \times 10^{-6} K^{-1}$, $\alpha_{zno} = 7.2 \times 10^{-6} K^{-6}$)[1,2], which helps reduce stress at the layer/substrate interface.
 - ✓ It is an economical choice.
 - ✓ The transparency of glass makes it ideal for optical characterization of films in the visible spectrum.
- b) Cleaning the substrate: Adherence and quality of thin films are mostly determined by their purity and surface condition. To clean the substrate surface, perform the steps below:
 - ✓ Use a pen with a diamond point to cut substrates.
 - ✓ Clean using a soap solution.
 - ✓ Rinse with distilled water.
 - ✓ Rinsing with acetone for 5 minutes.
 - ✓ Rinse with distilled water.
 - ✓ Rising with ethanol for 5 minutes
 - ✓ Drying with a dryer.

III.1.2.2 Preparation of solutions

In this study, four types of ZnO thin films were prepared: undoped ZnO, ZnO doped with 1% aluminum (AZO), ZnO doped with 1% cobalt (CZO), and ZnO co-doped with 1% aluminum and 1% cobalt (ACZO). The concentration of the solutions was maintained at 0.1 mol/l, The films were deposited on glass substrates using the spray pyrolysis technique. Zinc acetate [C₄H₆O₄Zn·2H₂O] was used as the precursor, while distilled water served as the solvent. Aluminium chloride hexahydrate [AlCl₃.6H₂O] and cobalt (II) chloride hexahydrate [CoCl₂·6H₂O] were employed as doping sources. Each solution was prepared by dissolving

the appropriate compounds in 20 mL of distilled water. The mixtures were magnetically stirred to ensure complete dissolution. A few drops of hydrochloric acid were added to enhance homogeneity and accelerate the dissolution process, resulting in clear and homogeneous precursor solutions ready for deposition.

III.1.2.3 Deposition of thin films

After preparing the four solutions (ZnO, AZO, CZO, ACZO), the glass substrates are carefully cleaned and weighed using a sensitive balance to record their initial mass. The substrates are then placed on a hot plate, and their temperature is gradually raised from room temperature to 400 °C using a precise temperature controller connected to a thermocouple for accurate monitoring and thermal regulation.

Once the desired temperature is reached, the spray bottle is filled with the ZnO solution using a clean syringe, and the substrates are sprayed for five minutes. The substrates are then left to cool gradually in air until they reach room temperature, allowing the film to adhere properly to the surface. After complete cooling, the substrates are reweighed to determine the change in mass, which is used to estimate the film thickness.

Properties of the used elements

Table (III-1) Physical and chemical properties of Zinc acetate, Aluminium chloride hexahydrate and Cobalt chloride hexahydrate

Materials Properties	Zinc acetate	Aluminium chloride hexahydrate	Cobalt chloride hexahydrate
Chemical formula	$\operatorname{Zn} C_4 H_6 O_4$. $2H_2 O$	$AlCl_3.6H_2O$	$CoCl_2.6H_2O$
Volumetric weight	1.73g /cm ³	$2.44 \mathrm{g}/\mathrm{cm}^3$	1.92 g/cm^3
Molecular weight	219.5g/ mol	241.43g/m	237,93g/mol
Melting temperature	237°C	192°C	86°C
Solubility	Soluble in water and methanol	Highly soluble in water	Highly soluble in water

❖ Experimental conditions: The following table outlines the experimental conditions used in the study

Table (III-2): Experimental conditions

	Doping	Substrate	Molarity of	Duration of	Distance the
Samples	concentration.	temperature	the solution	spraying	atomizer from the
		(° C)	(mol / l)	(min)	substrate (cm)
	(wt%)				
ZNO	unpoded				
AZO	1%Al				
CZO	1%Co	400	0.1	5	12
ACZO	1%Al;1%Co				

III.2 Results and discussions

III.2.1 Growth rate of the films

The growth rate was calculated by dividing the films thickness by the deposition time(5 minutes), we used the weight difference technique to calculate the thickness . Thickness and growth rate of our thin films (ZnO, AZO, CZO and ACZO) As shown in the following table

Table (III-3): Thickness and growth rate of ACZO thin films.

	ZNO	AZO	CZO	ACZO
t(nm)	520	480	390	150
Growth rate (nm /min)	104	96	78	30

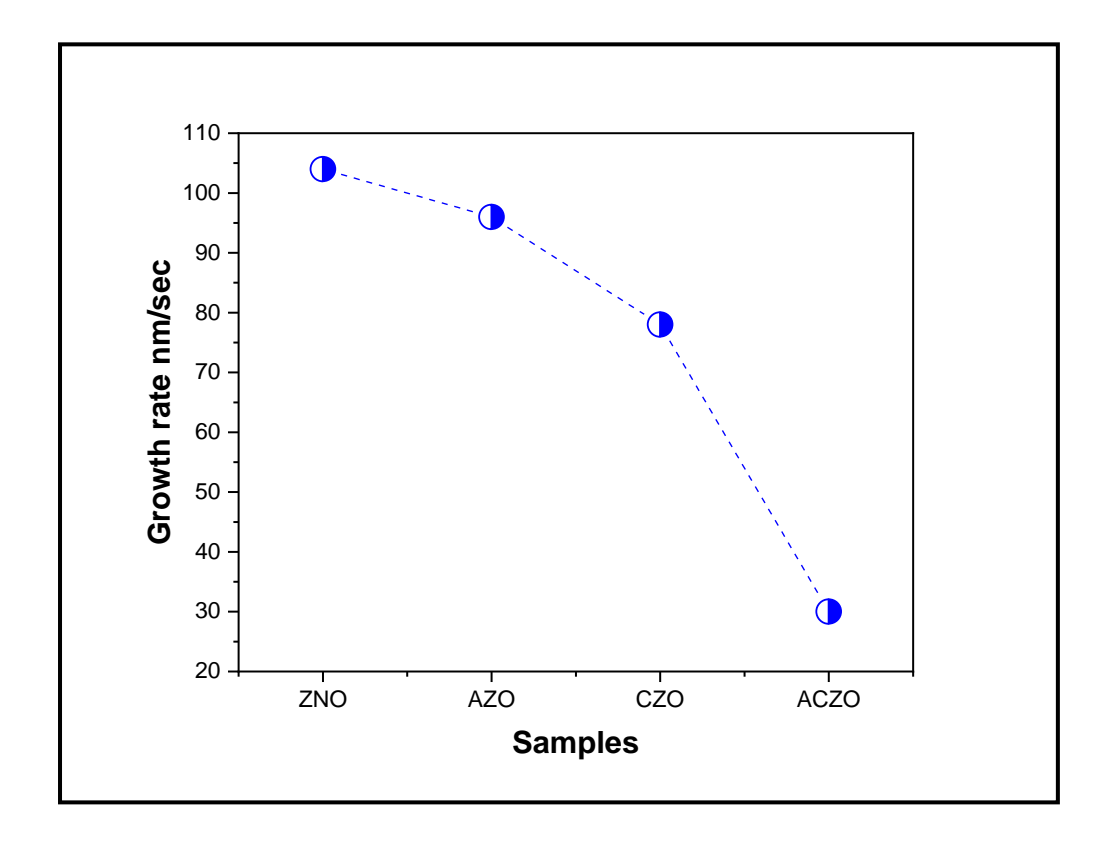


Figure III-2: Variation of growth rate ZnO / AZO / CZO / ACZO

Figure (III-2) presents the variation in thin film growth rate for different doping configurations. The undoped ZnO sample exhibited the highest growth rate, reaching 104 nm/min, indicating a rapid deposition of material onto the substrate. Upon doping with aluminum (AZO), the growth rate slightly decreased to 96 nm/min, suggesting a minor influence of Al³⁺ ions on the deposition kinetics [3].

The CZO sample, doped with cobalt, showed a further reduction in growth rate to 78 nm/sec, likely due to the incorporation of Co²⁺ ions affecting the crystal growth mechanism These incorporation can be attributed to the agglomeration which formed during the film growth.[4].

The co-doped ACZO sample exhibited the lowest growth rate of 30 nm/min, likely due to the simultaneous incorporation of Al³⁺ and Co²⁺ ions, which induce lattice distortions that hinder crystal growth and decrease nucleation efficiency.

III.2.2 Structural properties

III.2.2.1.X-ray Diffraction Spectrum (XRD)

X-ray diffraction results were obtained using the "Rigaku MiniFlex 600" device in the Thin Films and Their Applications Laboratory LPCMA, using CuK α radiation with a wavelength of 1.541874 Å. All samples were scanned within the angular range of 20° to 60°. Figure (III-3) shows the X-ray diffraction patterns of ZnO, AZO, CZO, and ACZO thin films.

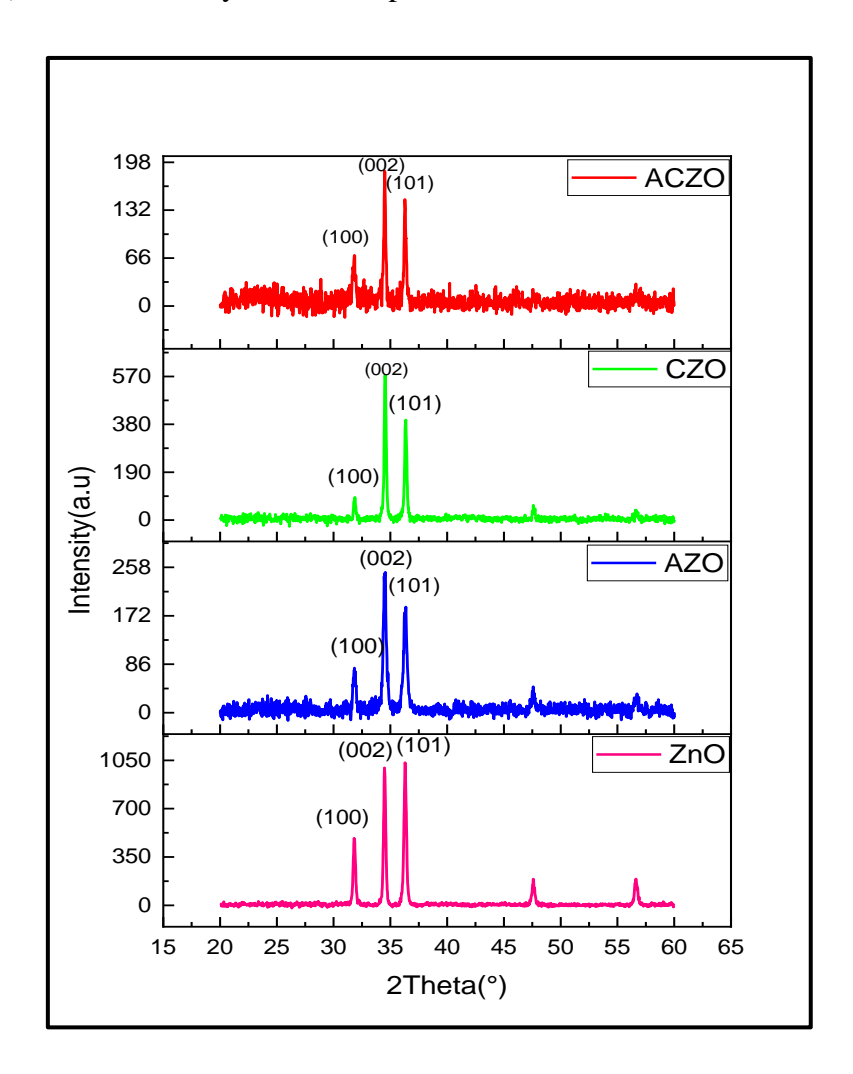


Figure III-3:X ray Diffractogram of thin films

The XRD spectra of ZnO, AZO, CZO, and ACZO films are presented in Figure (III-3) The (100), (002) and (101) diffraction peaks were observed. These peaks are in good agreement with the JCPDS reference file (No 36-1451) [5], which confirms the hexagonal structure of wurtzite type for all the elaborated layers and the polycrystalline structure, Sifei

Shao et al also found similar results in their study [6], observing the same peaks at these angles, confirming the regular hexagonal structure of the ZnO films. No peak belongs for any other phase which indicates the successful doping process and the singularity of the ZnO phase. This suggests that cobalt and aluminum doping did not affect the wurtzite ZnO crystal structure or its preferential c-axis orientation.

Additionally, minor peaks corresponding to the (102) and (110) planes appeared at 2θ angles of 47.57° and 56.57. The results indicate that Co^{2+} and Al^{3+} ions were replaced into Zn^{2+} ion sites or integrated into interstitial locations inside the ZnO lattice [7,8]. The intensity of the (100) and (101) peaks decreases with Al doping, while Co doping leads to an increase in the intensity of all peaks, particularly in the (002) plane [9].

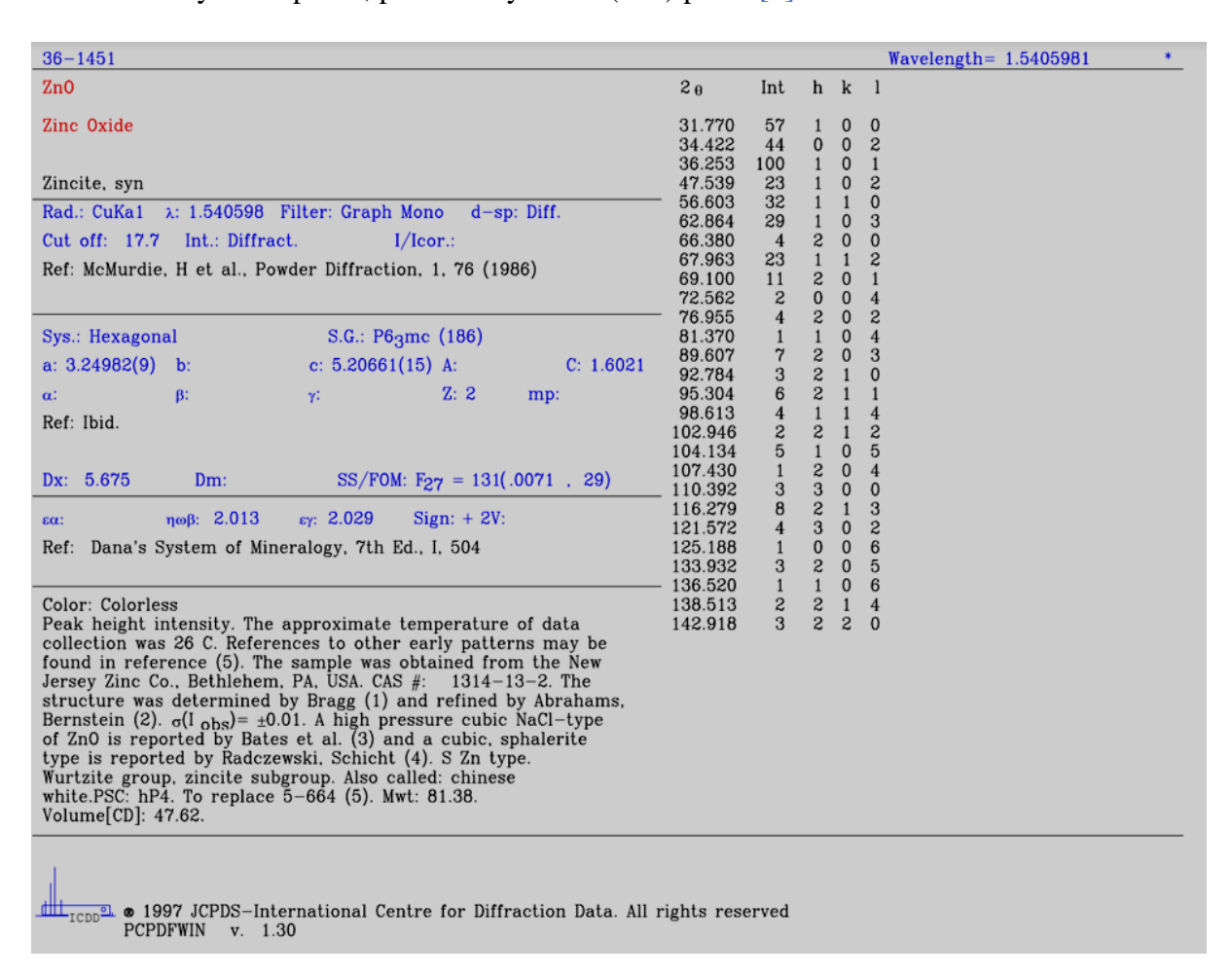


Figure III-4: JCPDS NO. 36-1451 folder

From Figure (III-5), it can be seen a slight shift in the position peak (002) towards a higher 2θ angle with Co and Al doping compared to the bulk values ($2\theta = 34.42$) attributed to the substitution of Zn^{2+} ions (0.74 Å) with smaller Co^{2+} (0.65 Å) and Al^{3+} (0.54 Å) ions. This

ionic replacement induces lattice contraction, particularly along the c-axis, resulting in reduced interplanar spacing. According to Bragg's Law, this contraction leads to an increase in the diffraction angle, indicating the presence of compressive lattice strain. Similar observations were reported by C.-L. Tsai et al., who linked the shift to variations in dopant concentration. C.-L. Tsai et al [10] reported that a slight shift in thepeak position of the (002) plane was observed, which is due to the variation in the doping of both cobalt and aluminum in the films [11,12].

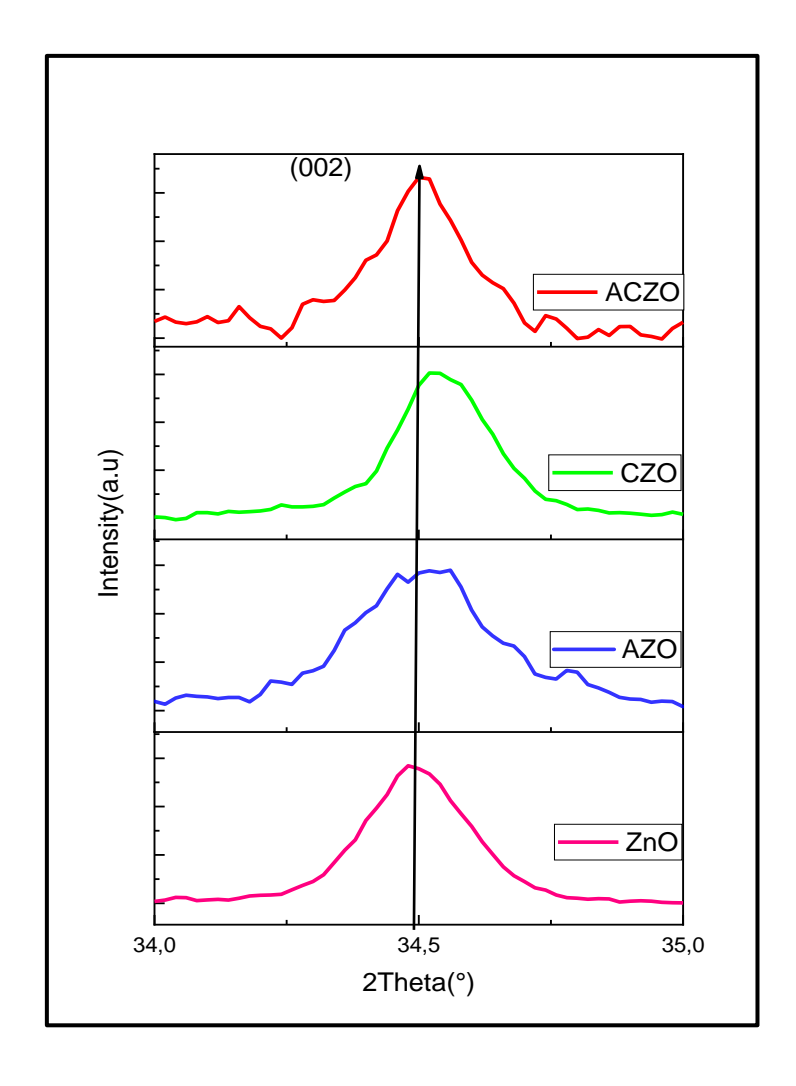


Figure III-5 : XRD patterns of (002) diffraction peak.

III.2.2.2. Crystallite size

The crystallite size of ZnO thin films varies significantly with the type of doping, as calculated using the Scherrer equation (Equation II-7).

The variations in crystallite size as a function of dopant type are shown in Figure (III-6). It was found that the undoped zinc sample exhibited a crystallite size of 35.82 nm, which is consistent with previous studies [13]. Al-doping reduced the crystallite size to 28.99 nm due to lattice strain induced by the smaller Al³⁺ ions, consistent with findings by T. Ratana et al [14]. In contrast, Co-doped ZnO (CZO) showed the largest crystallites (46,11 nm) as observed by Anfal Ali Shakir [15]. This can be attributed to the closer ionic radius of Co²⁺ (0.65 Å), resulting in improved crystallinity, as confirmed by the XRD patterns. Co-doping with Al and Co yielded an intermediate crystallite size (35.87 nm), reflecting a balance between grain growth promotion and suppression.

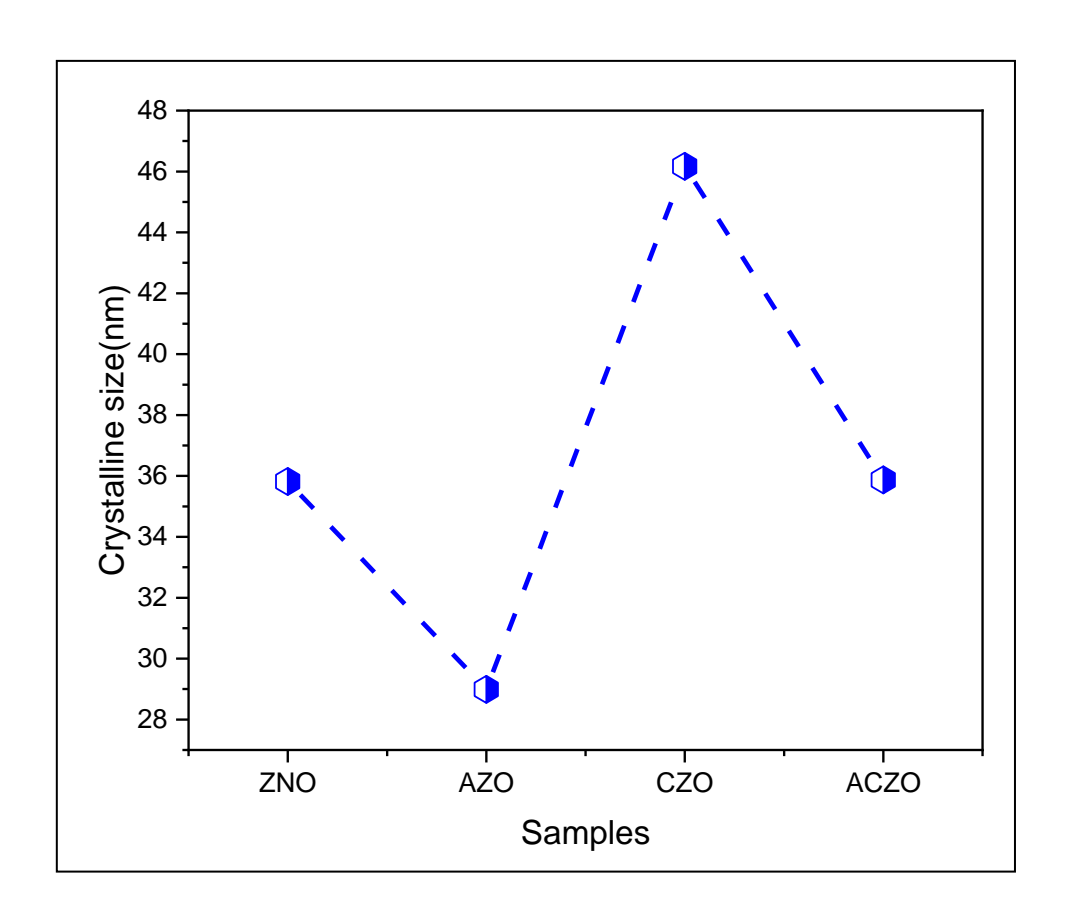


Figure III-6: Variation in the crystallite size of ZnO, AZO, CZO, and ACZO samples.

Table (III-4): crystallite size of thin films

samples	hkl	2θ (°)	D(nm)	$D_{moy}(nm)$
EN 10	(100)	31,82	31,0570	
ZNO	(002)	34,49	31,0571	35,8287
	(101)	36,29	44,8583	,
AZO	(100)		22,4290	
	(002)	34,51	28,8360	28,997
	(101)	36,29	33,6342	
CZO	(100)	31,79	40,3677	
	(002)	34,52	40,3292	46,1162
	(101)	36,32	57,6518	
ACZO	(100)	31,80	33,6341	
-1023	(002)	34,50	33,6379	35,8787
	(100)	36,28	40,3679	

III.2.2.3 Dislocation density, strain and stress

The findings of crystallite size (D), dislocation density (δ) strain (ϵ) and internal stress (σ) are presented in Table (III-5); Fig (III-7) As observed the inverse relation between both parameters (crystalline size et strain). the CZO thin films exhibited a high crystallite size accompanied by minimal strain. This indicates an enhancement in crystalline characteristics and fewer surface defects. As explained by XRD results. This phenomenon is ascribed to the compressive strain induced by the disparity in ionic radii among the dopant and zinc ions, resulting in defect generation within the crystals.[16]. These values indicate significant distortions in the crystal lattice [17,18].

Samples	D (nm)	δ (x 10^{14} line/ m^2)	$\epsilon imes 10^{-4}$	σ GPa
ZnO	35,8287	8,566	10.1	0,446
AZO	28,997	13,57	12,4	0,581
CZO	46,1162	5,027	7,80	0,625
ACZO	35,8787	6,36	10.08	0,536

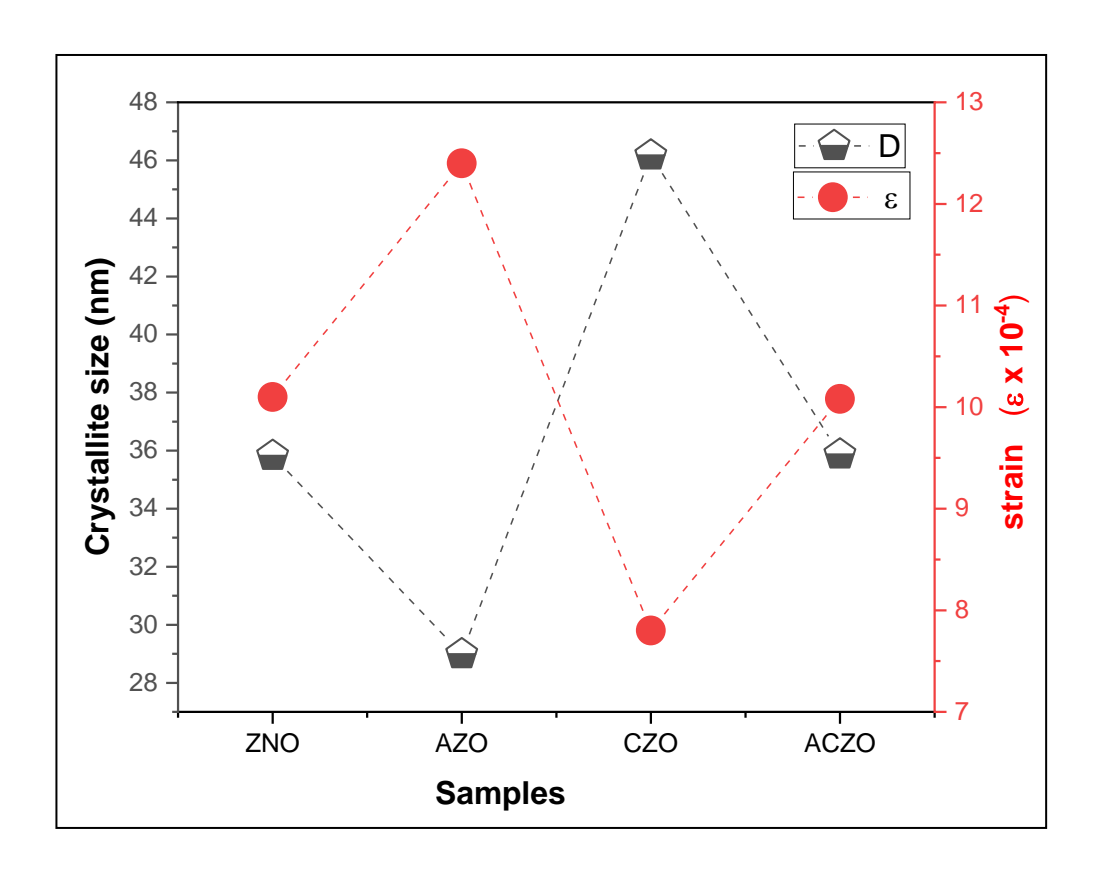


Figure III -7 : Variation in the crystallite size and strain of ZnO, AZO, CZO, and ACZO samples.

III.2.2.4 lattice parameters

Table (III-6) presents the experimental values of the lattice parameters a and c and the c/a ratio for thin film samples (ZnO, AZO, CZO, ACZO), calculated based on equations (II-5 and II-6) described in Chapter II. The c lattice parameter ranges between 5.196 Å and 5.192 Å, while *a* ranges between 3.249 Å and 3.244 Å, as shown in Figure (III-8) and Figure (III-9).

It is worth noting that other studies have reported very similar values [19,20]. It was observed that the c/a ratio gradually decreases across the samples gradually decreases compared to the undoped sample ZnO. ranging from 1.602 1.598, indicating lattice strain caused by doping with elements such as Al and Co (see table III-6and figure III-8), which leads to slight distortions in the lattice dimensions. This variation is attributed to compressive strain within the crystal structure, as illustrated in Figure III-5[21].

Table (III-6) lattice parameters of thin films

samples	a (Å)	a_0	c_0	c(Å)	c/a	
ZnO	3,244	3,25		5,196	1,602	
AZO	3,249		3,25	5,21	5,193	1,598
CZO	3,247				5,192	1,599
ACZO	3,245			5,194	1,600	

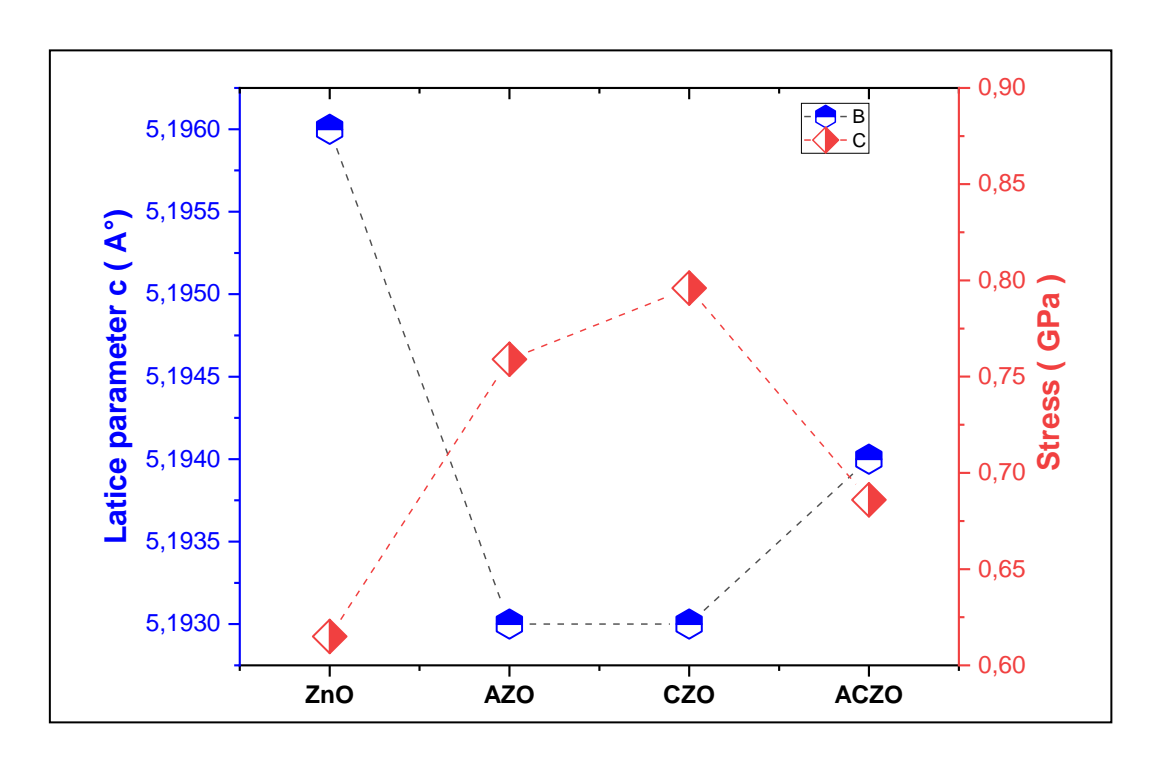


Figure III-8: Variation in Lattice Parameters c and stress in ZnO, AZO, CZO, and ACZO Samples

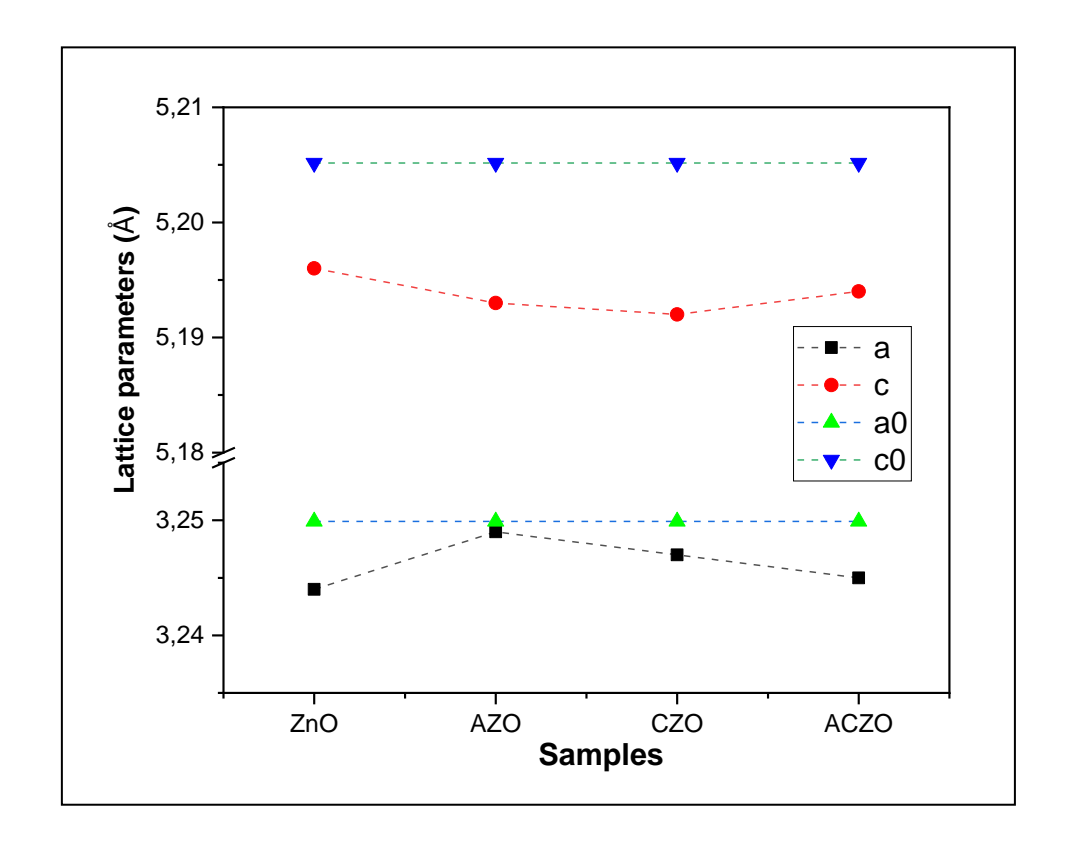


Figure III-9 : Lattice parameters *a* and c of ZnO/AZO/CZO/ACZO

III.2.3. Optical properties

III.2.3.1. Transmittance spectra

In this study, the ASCOV-770UV-VIS spectrophotometer was used to measure the optical transmittance spectra of thin films within the wavelength range of 300 to 900 nm, as shown in Figure III.10. The graph illustrates the relationship between optical transmittance (T%) and wavelength (λ) for ZnO, AZO, CZO and ACZO.

The results show that all thin films exhibit low transmittance in the ultraviolet region (300–400 nm), and the absorption edges shift to longer wavelengths when doped with Al and Co. In the visible range (400–800 nm), the optical transmittance generally increases, typically ranging between approximately 80% and 95%, which is consistent with values reported in other studies [22, 23]. At a wavelength of 550 nm, the transmittance of ZnO is approximately 87.402%, that of the AZO sample is about 90.57%, the CZO sample reaches 89.26%, while the ACZO shows the highest transmittance at 93.37%.

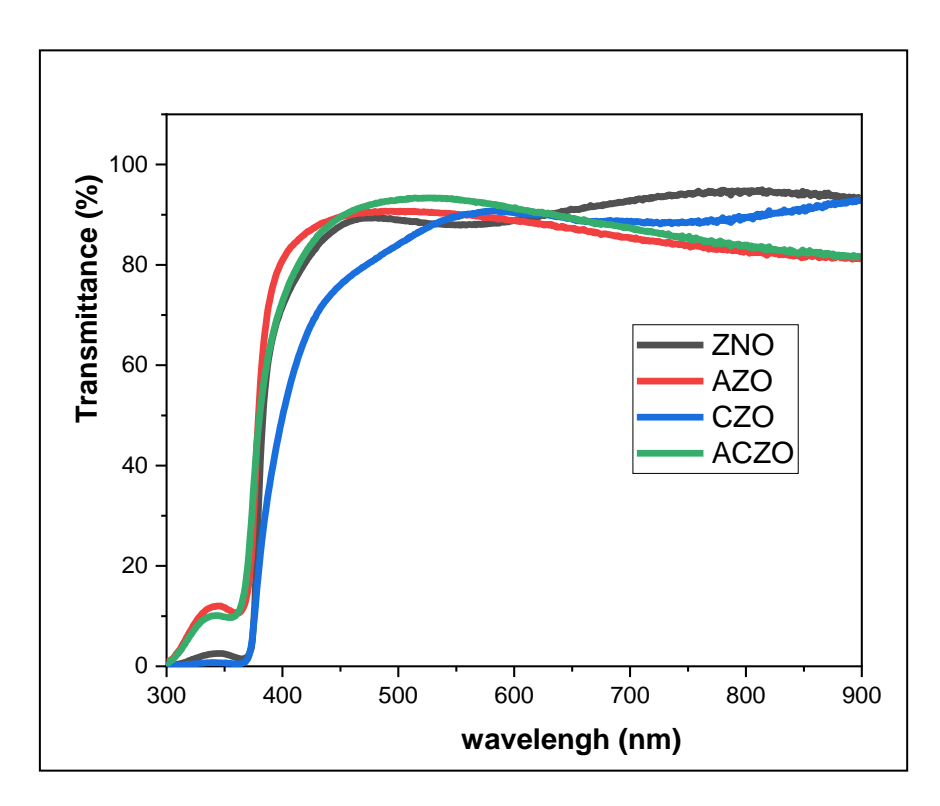


Figure III- 10: Transmittance spectra of ZnO/AZO/CZO/ACZO thin films

It can be observed from Figure (III-11) that transmittance at 550nm is inversely proportional to the thickness, similar observation has been found by researchers [24,25]. As it is known the transmittance is depending on thickness of samples according to Beer-Lambert law (see chap. II).

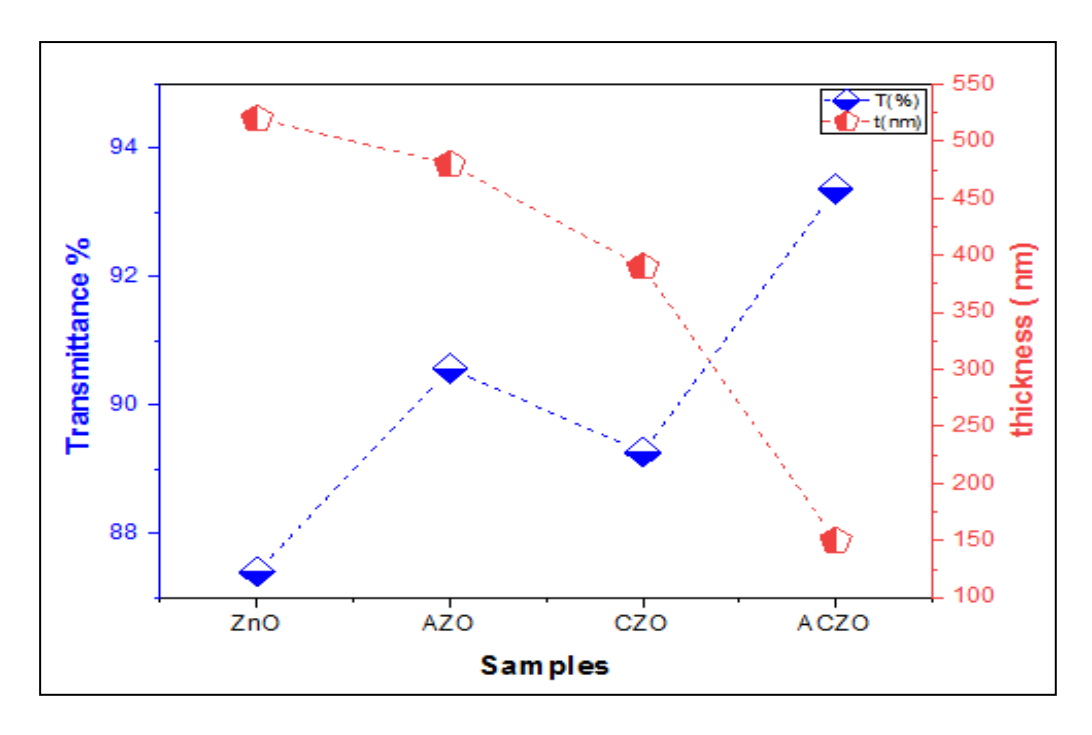


Figure III-11: Variation of average transmittance and thikness of thin films at 550nm

III.2.3.2. Band gap energy and Urbach energy

The optical band gap of ZnO films was determined based on UV-VIS transmission measurements by plotting $(\alpha h v)^2$ as a function of h v, using the equation II-14 presented in Chapter II, as shown in Figure III-12

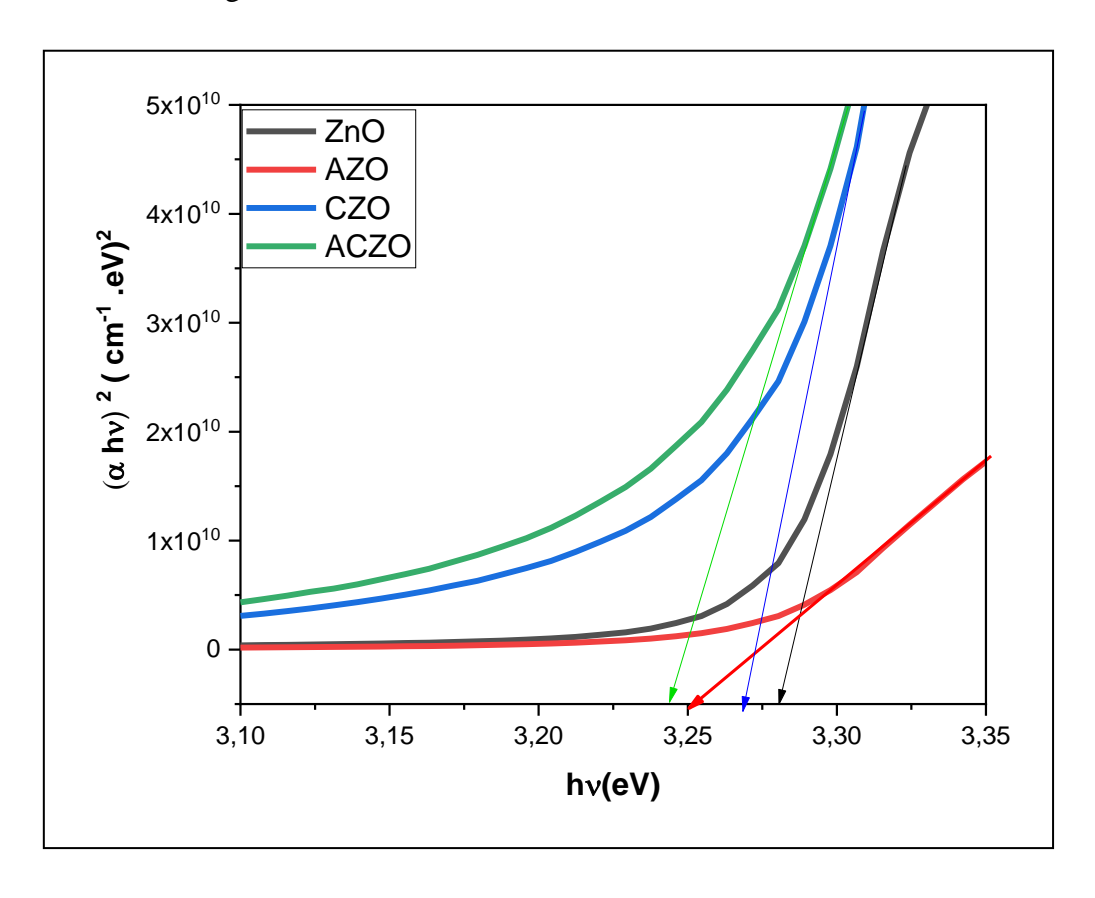


Figure III-12: The plot $(\alpha hv)^2$ versus (hv) for the calculation of the optical band gap energy Eg

The results in table III-7 indicate that the optical band gap (Eg) decreases upon doping ZnO with aluminum and cobalt, compared to undoped ZnO (3.281 eV). The recorded values are 3.253 eV, 3.268 eV, and 3.244 eV for the different samples AZO, CZO and ACZO respectively, Similar values have been reported in previous studies. [26-29]

In the figure III-13, an inverse relationship is observed between optical band gap and Urbach energy. The incorporation of dopants into ZnO thin films results in a decrease in the optical band gap and an increase in the Urbach energy, reflecting the introduction of structural disorder and localized defect states. The undoped ZnO sample exhibits a band gap of 3.281 eV and a low Urbach energy of 0.341 eV, while doped samples show reduced band gaps to

3.244 eV and increased Urbach energies to 0.401 eV. This confirms that dopant incorporation distorts the lattice and creates localized states that modify the electronic structure [28].

Moreover, Table (III-7) displays the refractive index values for ZnO, AZO, CZO, and ACZO thin films the changes in the refractive index resulting from doping, calculated using the **Ravindra**, **Herve and Vandamme** models, which significantly affect the optical and transport properties of ZnO thin films [30].

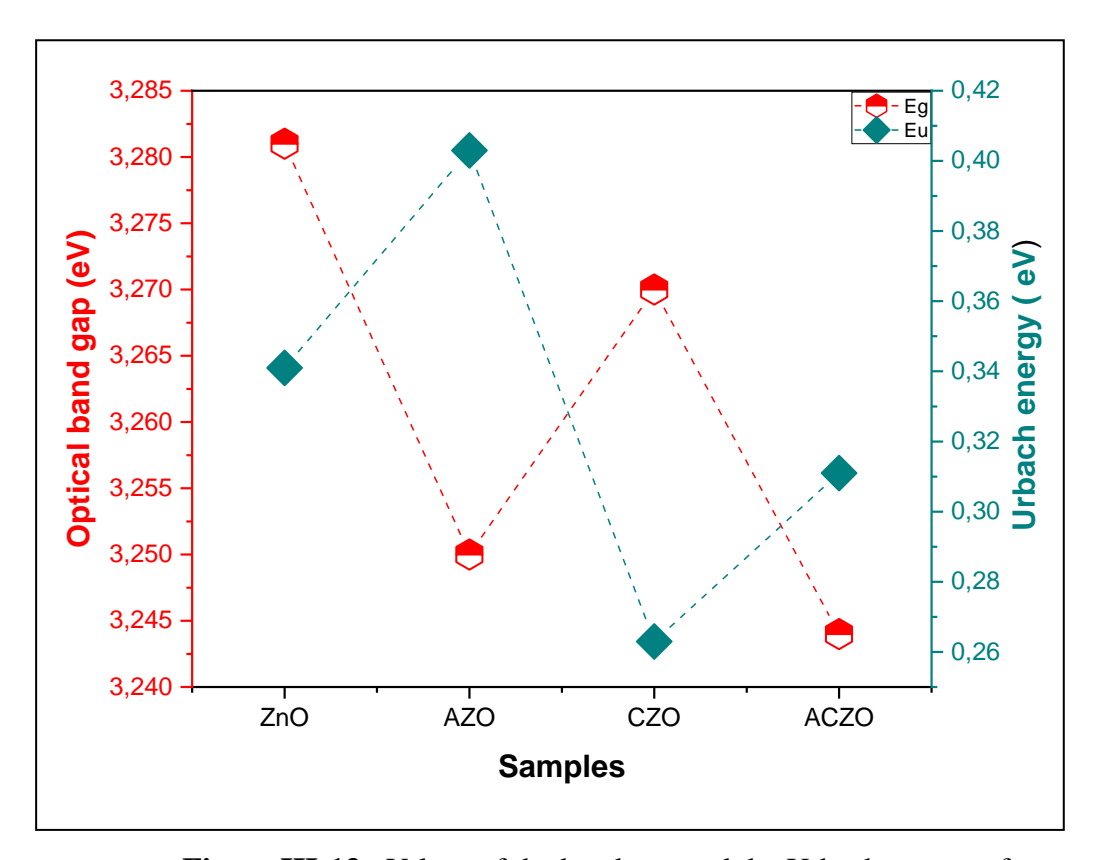


Figure III-13: Values of the band gap and the Urbach energy of ZnO/AZO/CZO/ACZO thin films.

Table (III-7) Optical properties of thin films

Samples	Thickness	Transmittance	Optical	*		Refractive index	
	(nm)	(%) at550	band gap	energy	Herve and	Ravindra	
			(eV	(eV)	Vandamme		
ZNO	520	87,402	3,281	0,341	2,267	2,049	
AZO	480	90,57	3,253	0,401	2,276	2,069	
CZO	390	89,26	3,268	0,263	2,270	2,056	
ACZO	150	93,37	3,244	0,311	2,278	2,072	

III.2.3. Electrical properties

The electrical properties of ZnO, AZO, CZO, and ACZO thin films were studied using the four-point probe technique. The absence resistivity value for the ACZO sample is likely due to issues during deposition or measurement with the four-point probe, which may have affected the accuracy of the electrical properties. The resistivity values and figure of merit are shown in the table III-8.

Sample	Thickness	T (%)	R_s	Resistivity	Conductivity	(FOM)
S	(x 10 ⁷ cm)		(Ω/sheet)	(Q.cm)	(Ω.cm) ⁻¹	(Ω^{-1})
ZnO	520	87,402	156.94x10 ⁶	$8,16 \times 10^3$	1.225x10 ⁻⁴	$1,65 \times 10^{-9}$
AZO	480	90,57	8.78×10^6	$4,21 \times 10^2$	2.375 x 10 ⁻³	4.23×10^{-8}
CZO	390	89,26	542.75	$2,11 \times 10^{-2}$	47.397	5.91×10^{-4}
ACZO	150	93,37				

The following figure illustrates the variation in electrical resistivity and crystalline size of undoped and doped ZnO thin films (ZnO. AZO and CZO):

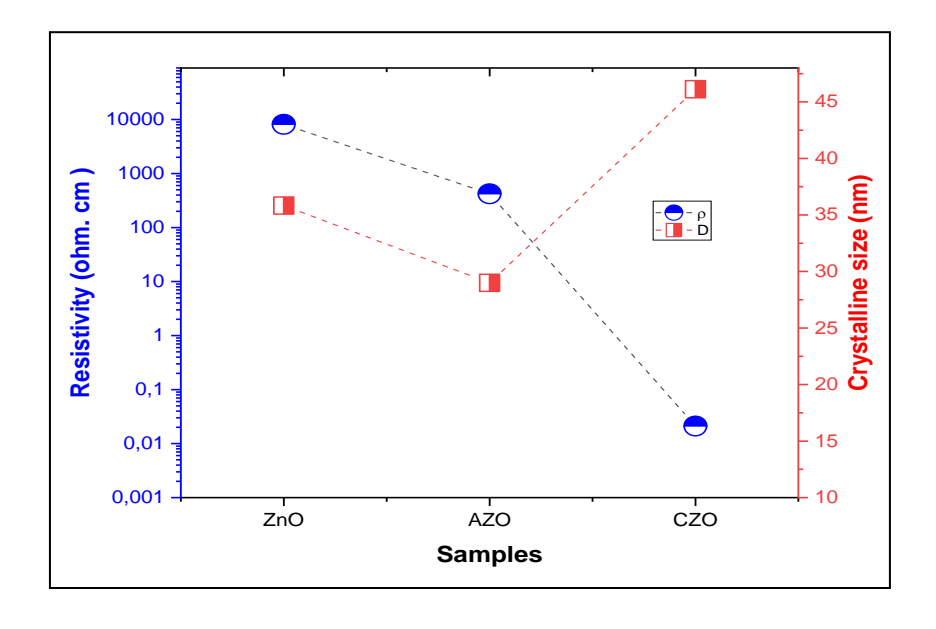


Figure III- 14: Resistivity and Band gap of ZnO/AZO/CZO thin films

The results for ZnO, AZO, and CZO show that resistivity decreases progressively with doping (from 8160 to 0.021 Ω ·cm), while the cristalline size increases (from 28,99 nm to 46,1162 nm), the decrease in resistivity in the CZO sample can be attributed to the increase in grain size, which reduces the number of grain boundaries within the crystal structure. This reduction decreases the density of structural defects, as illustrated in Figure III.14. Consequently, the improvement in crystalline quality enhances the carrier mobility, which directly affects the electrical properties of the film. This effect has been demonstrated in previous studies [31, 32].

The quality factor (Q) summarizes both optical and electrical properties in ZnO films (see figure III.15). A higher Q, as seen in CZO, indicates better crystallinity, higher conductivity, and improved light transmission, making it ideal for optoelectronic use

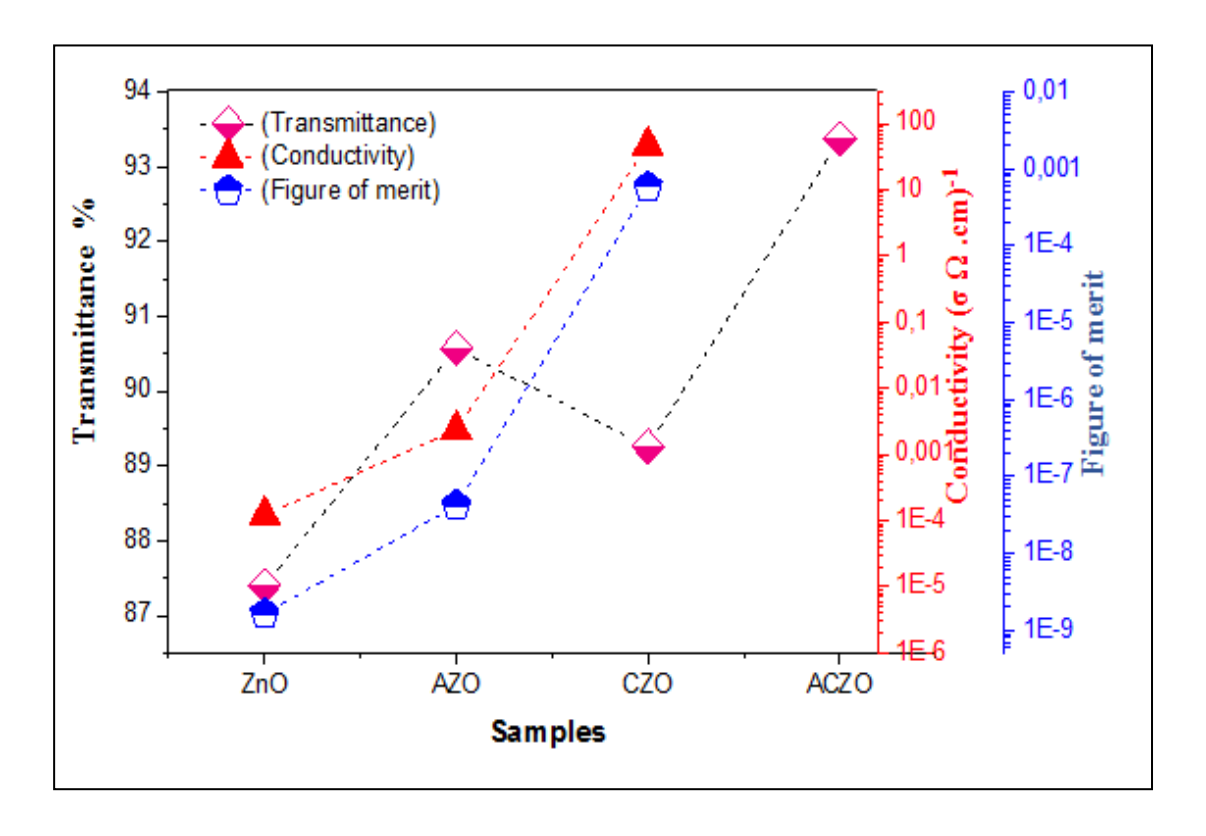


Figure III -15: Variation of transmittance, conductivity, and quality factor of thin film

References

- [1] Bouhssira, N. (2013). Élaboration des films minces d'oxyde de zinc par évaporation et par pulvérisation magnétron et étude de leurs propriétés [Thèse de doctorat en sciences, Université Constantine 1]
- [2] Othmane, M. (2010). dépôt et caractérisation des couches minces d'oxyde de zinc par spray pyrolyse ultrasonique (Doctoral dissertation, Université Mohamed Khider-Biskra).
- [3] Zhai, C. H., Zhang, R. J., Chen, X., Zheng, Y. X., Wang, S. Y., Liu, J., ... & Chen, L. Y. (2016). Effects of Al doping on the properties of ZnO thin films deposited by atomic layer deposition. Nanoscale research letters, 11, 1-8.
- [4] Salah, A., Saad, A. M., & Aboud, A. A. (2021). Effect of Co-doping level on physical properties of ZnO thin films. Optical Materials, 113, 110812.
- [5] Benkheta, Y. (2019). Elaboration and characterization of thin layers of zinc oxide (ZnO) deposited by ultrasonic spray for photovoltaic and optoelectronic applications (Doctoral dissertation, University Mohamed Khider of Biskra).
- [6] Shao, S., Jia, P., Liu, S., & Bai, W. (2008). Stable field emission from rose-like zinc oxide nanostructures synthesized through a hydrothermal route. Materials Letters, 62(8-9), 1200-1203.
- [7] Marinov, G., Georgieva, B., Vasileva, M., & Babeva, T. (2023). Study of structure, morphology and optical properties of cobalt-doped and Co/Al-co-doped ZnO thin films deposited by electrospray method. Applied Sciences, 13(17), 9611.
- [8] Caglar, Y. (2013). Sol–gel derived nanostructure undoped and cobalt doped ZnO: Structural, optical and electrical studies. Journal of alloys and Compounds, 560, 181-188.
- [9] Banerjee, P., Lee, W.-J., Bae, K.-R., Lee, S. B., & Rubloff, G. W. (2010). Structural, electrical, and optical properties of atomic layer deposition Al-doped ZnO films. Journal of Applied Physics, 108(4), 043504
- [10] Tsai, C. L., Lin, Y. J., Liu, C. J., Horng, L., Shih, Y. T., Wang, M. S., ... & Chang, H. C. (2009). Structural, electrical, optical and magnetic properties of Co0. 2AlxZn0. 8– xO films. Applied surface science, 255(20), 8643-8647.

- [11] Lung, C., Toma, M., Pop, M., Marconi, D., & Pop, A. (2017). Characterization of the structural and optical properties of ZnO thin films doped with Ga, Al and (Al+ Ga). Journal of Alloys and Compounds, 725, 1238-1243.
- [12] Liu, Z., & Yang, P. (2018). Optoelectronic performances on different structures of Al-doped ZnO. Journal of the American Ceramic Society, 101(12), 5615-5626.
- [13] Wasly, H. (2018). X-ray analysis for determination the crystallite size and lattice strain in ZnO nanoparticles. Journal of Al-Azhar University Engineering Sector, 13(49), 1312-1320.
- [14] Ratana, T., Amornpitoksuk, P., & Suwanboon, S. (2009). The wide band gap of highly oriented nanocrystalline Al doped ZnO thin films from sol–gel dip coating. Journal of Alloys and Compounds, 470(1-2), 408-412.
- [15] Shakir, A. A. (2017). Structural and optical characterization of cobalt-doped zinc oxide thin films deposited by chemical spray pyrolysis. Journal of Kufa-Physics, 9(2), 32-40.
- [16] Sun, H., Chen, S. C., Wang, C. H., Lin, Y. W., Wen, C. K., Chuang, T. H., ... & Dai, M. J. (2019). Electrical and magnetic properties of (Al, Co) co-doped ZnO films deposited by RF magnetron sputtering. Surface and Coatings Technology, 359, 390-395.
- [17] Li, K., Wei, Z., Zhu, X., Zhao, W., Zhang, X., & Jiang, J. (2018). Microstructure and optical properties of ZnO nanorods prepared by anodic arc plasma method. Journal of Applied Biomaterials & Functional Materials, 16(1_suppl), 105-111.
- [18] Yadav, S., Singh, M., Verma, D. K., & Jaiswar, G. (2017). X-ray diffraction study of the effects of dopant on the lattice strain of zinc oxide nanoparticles. Adv. Nanomater. Technol. Energy Sect, 1, 73-89.
- [19] Wang, F. H., & Chang, C. L. (2016). Effect of substrate temperature on transparent conducting Al and F co-doped ZnO thin films prepared by rf magnetron sputtering. Applied surface science, 370, 83-91.
- [20] Thomas, A., & Sivaperuman, K. (2025). Carbon and cobalt co-doped ZnO thin films for highly sensitive and selective ammonia detection at room temperature. Materials Advances, 6(2), 629-640.

- [21] Wojnarowicz, J., Chudoba, T., Gierlotka, S., Sobczak, K., & Lojkowski, W. (2018). Size control of cobalt-doped ZnO nanoparticles obtained in microwave solvothermal synthesis. Crystals, 8(4), 179.
- [22] Cisneros-Contreras, I. R., López-Ganem, G., Sánchez-Dena, O., Wong, Y. H., Pérez-Martínez, A. L., & Rodríguez-Gómez, A. (2023). Al-doped ZnO thin films with 80% average transmittance and 32 Ohms per square sheet resistance: A genuine alternative to commercial high-performance indium tin oxide. Physics, 5(1), 45-58.
- [23] Lai, L. W., & Lee, C. T. (2008). Investigation of optical and electrical properties of ZnO thin films. Materials Chemistry and Physics, 110(2-3), 393-396.
- [24] Malandrino, G., Blandino, M., Fragala, M. E., Losurdo, M., & Bruno, G. (2008). Relationship between nanostructure and optical properties of ZnO thin films. The Journal of Physical Chemistry C, 112(26), 9595-9599.
- [25] Chen, J., Chen, D., He, J., Zhang, S., & Chen, Z. (2009). The microstructure, optical, and electrical properties of sol–gel-derived Sc-doped and Al–Sc co-doped ZnO thin films. Applied Surface Science, 255(23), 9413-9419.
- [26] Joshi, S., & Leela, S. (2021). Studies on structural and optical properties of Cobalt doped ZnO thin films prepared by Sol-gel spin coating technique. Materials Today: Proceedings, 43, 3166-3168.
- [27] Marinov, G., Georgieva, B., Vasileva, M., & Babeva, T. (2023). Study of structure, morphology and optical properties of cobalt-doped and Co/Al-co-doped ZnO thin films deposited by electrospray method. Applied Sciences, 13(17), 9611.
- [28] Djaaboube, H., Mammeri, A., Bouachiba, Y., Taabouche, A., Bouabellou, A., Serrar, H., ... & Rahal, B. (2022). Optical properties and complex refractive index of Co-doped ZnO waveguide thin films elaborated by spray pyrolysis. Journal of Materials Science: Materials in Electronics, 33(20), 16056-16065.
- [29] Eisa, M. H., & Faraj, M. G. (2022). Optical properties of Al-doped zinc oxide (AZO) thin films with PLD technique. Digest Journal of Nanomaterials and Biostructures, 17(3), 705–714

- [30] Hamani, N., Bourhefir, R., Hafaifa, L., Bennaceur, K., & Berramdane, F. (2024). Influence of Al and Mg co-doping on structural and optical properties of ZnO thin films deposited by spray pyrolysis. Journal of Optics, 1-11.
- [31] Maffei, R. M., di Bona, A., Sygletou, M., Bisio, F., D'Addato, S., & Benedetti, S. (2023). Suppression of grain boundary contributions on carrier mobility in thin Al-doped ZnO epitaxial films. Applied Surface Science, 624, 157133.
- [32] Khan, M. I., Bhatti, K. A., Qindeel, R., Alonizan, N., & Althobaiti, H. S. (2017). Characterizations of multilayer ZnO thin films deposited by sol-gel spin coating technique. Results in physics, 7, 651-655.

General conclusion

This study focused on the preparation and characterization of ZnO thin films doped with aluminum, cobalt, and co-doped with both (Al-Co), using the Pneumatic Spray Pyrolysis (PSP) technique. The aim was to investigate the effect of individual and co-doping on the structural, optical and electrical properties of the films. The analysis of the properties of these samples was carried out by different characterization methods. In this context, we carried out structural characterizations by X-ray diffraction (XRD), optical by UV-VIS spectrometry, the FT-IR spectra were obtained with a Fourier transform infrared spectrometer and finally the electrical characterization by four-point measurement.

Four samples were prepared by varying the type of doping (ZnO, AZO, CZO and ACZO), while maintaining the concentration of both cobalt and aluminum fixed at 1%. Based on the results obtained from the various characterizations and the corresponding discussions, the following conclusions can be drawn:

The prepared thin films were crystallized in the wurtzite phase, with preferred orientations along the (002), (101), and (100) planes, and the presence of secondary orientations, indicating that the films are polycrystalline. Upon doping with cobalt, an increase in crystallite size and peak intensity was observed, which led to an improvement in the crystallinity of the films. This indicates that cobalt doping enhances the crystal quality of ZnO.

In addition, all the thin films exhibited high transparency in the visible range, with transmittance values approximately between 85% and 95%. The ACZO sample (co-doped with Al and Co) showed a high optical transmittance of around 93%, reflecting the high quality of the prepared films. Moreover, the optical band gap (Eg) was observed with doping, ranging from 3.244 to 3.281 eV. Notably, the highest band gap value was recorded after cobalt doping CZO where it reached 3.26 eV.

.

The CZO thin films also recorded the lowest electrical resistivity, around $2{,}11\times 10^{-2} \,(\Omega{,}\text{cm})$ at a cobalt concentration, along with the highest figure of merit, whichreached $5{,}91\times 10^{-4} \,(\Omega^{-1})$, reflecting the excellent performance of these films.

In summary, it can be concluded that cobalt concentration plays a fundamental role in enhancing the structural, optical, and electrical properties of ZnO thin films. Further research on CZO films would be beneficial, especially regarding their use in the photovoltaic field, with a focus on whether increasing the cobalt content could lead to further improvements in conductivity and optical transmittance

Effect of Al, Co, and Al/Co co-doping on the properties of ZnO thin films prepared via Pneumatic Spray Method

Abstract

The objective of this work is the deposition and characterization of zinc oxide (ZnO) thin films doped with aluminum (Al), cobalt (Co), and co-doped with both elements (Al-Co). The films were deposited using the pneumatic spray pyrolysis technique, and the effect of doping type on the structural, optical, and electrical properties of the prepared samples was investigated. To analyze and evaluate the properties of the films, several characterization techniques were employed, including: X-ray diffraction (XRD) to determine the crystalline structure UV-Visible spectroscopy to assess optical properties, and four-point probe measurements to evaluate electrical resistivity. The results showed that doping with cobalt (Co) led to significant improvements in the properties of the ZnO films. Specifically, it enhanced crystallinity, increased transparency in the visible range, and improved electrical performance compared to undoped films, Al-doped films, and codoped films, We found that this sample has the best crystallization, and a uniform surface, and high transparency in the visible range (89%), with a band gap 3.26 eV, in addition to a good figure of merit (5.91 $\cdot 10^{-4}\Omega^{-1}$).

Keywords: ZnO, cobalt doping, aluminum doping, co-doping, thin films, properties

Effet du dopage par Al, Co et du co-dopage Al/Co sur les propriétés des films minces de ZnO préparés par la méthode de pulvérisation pneumatique.

Resumé

L'objectif de ce travail est le dépôt et la caractérisation des films minces d'oxyde de zinc (ZnO) dopés à l'aluminium (Al), au cobalt (Co) et co-dopés avec les deux éléments (Al-Co). Les films ont été déposés en utilisant la technique de spray pneumatique pyrolyse , l'effet du type de dopage sur les propriétés structurales, optiques et électriques des échantillons préparés a été étudié. Pour analyser et évaluer les propriétés des films, plusieurs techniques de caractérisation ont été employées, notamment :La diffraction des rayons X (DRX) pour déterminer la structure cristalline, La spectroscopie UV-Visible pour évaluer les propriétés optiques, Et la méthode à quatre pointes pour mesurer la résistivité électrique. Les résultats ont montré que le dopage au cobalt (Co) a conduit à des améliorations significatives des propriétés des films de ZnO. Plus précisément, il a permis d'améliorer la cristallinité, d'augmenter la transparence dans le domaine visible et d'améliorer les performances électriques par rapport aux films non dopés, dopés à l'aluminium, et co-dopés. Nous avons constaté que cet échantillon présente la meilleure cristallisation, une surface uniforme et une haute transparence dans le domaine visible (89%), avec une bande interdite de 3,26 eV, en plus d'un bon facteur de mérite (5,91 × $10^{-4} \Omega^{-1}$).

Mots-clés: ZnO, dopage au cobalt, dopage à l'aluminium, co-dopage, films minces, propriétés.

تأثير التطعيم بالألمنيوم(Al) الكوبالت (Co) ، التطعيم المزدوج (Al/Co)على خصائص الأغشية الرقيقة لـ ZnO المحضرة بالألمنيوم(Al) باستخدام طريقة الرش الهوائي المضغوط

ملخص

هدف هذا العمل هو ترسيب وتوصيف الأغشية الرقيقة من أكسيد الزنك (ZnO) المطعّمة بالألمنيوم(Al) ، والكوبالت(Co) ، والتطعيم المزدوج بكلا العنصرين .(Al-Co) تم ترسيب هذه الأغشية باستخدام تقنية التحلل بالرش بالهواء المضغوط، وتمت دراسة تأثير نوع التطعيم على الخصائص البنيوية والبصرية والكهربائية للعينات المحضرة ولتحليل وتقبيم خصائص هذه الأغشية، تم استخدام عدة تقنيات من بينها:حيود الأشعة السينية (XRD) لتحديد البنية البلورية، التحليل الطيفي بالأشعة فوق البنفسجية المرئية (Co) لتقييم الخصائص البصرية، و القياس بأربع نقاط لقياس المقاومة الكهربائية أظهرت النتائج أن التطعيم بالكوبالت (Co) أدى إلى تحسينات كبيرة في خصائص أغشية OZ محسن من درجة التبلور، وزاد من الشفافية في النطاق المرئي، كما حسن الأداء الكهربائي مقارنةً بالأغشية غير المطعّمة، والمطعّمة بالألمنيوم فقط والتطعيم المزدوج. ووجدنا أن هذه العينة تقدم أفضل تبلور، وسطح موحد وشفافية عالية في النطاق المرئي (89٪)، مع فجوة نطاق تبلغ 26. 3 إلكترون فولط، بالإضافة إلى عامل الجودة الجيد (5,91 × 10-1-20).

الكلمات المفتاحية: ZnO، التطعيم بالكوبالت، التطعيم بالألمنيوم، التطعيم المزدوج، الأعشية الرقيقة، الخصائص.

REPUBLIQUE ALGERIENNE DEMOCRATIQUE ET POPULAIRE MINISTERE DE L'ENSEIGNEMENT SUPERIEUR ET DE LA RECHERCHE SCIENTIFIQUE UNIVERSITE MOHAMED KHIDER - BISKRA



الجمعورية الجزائرية الديمقراطية الشعبية وزارة التعليم العالي والبحث العلمي جامعة محمط خيض يسكرة

كلية العلوم الحقيقة

Faculté des SE

Département des Sciences de la matière

Filière: Physique



تصريح شرفي

فكس بالالتزام بقواعد النزاهة العلمية لإنجاز بحث

(ملحق القرار 1082 المؤرخ في 2021/12/27)

	الممضي اسفله،
	السيد(ة): جرد سي سما يسيل
الصفة: طالب سنة تنا سية ساستر	تخصص عِبْن بإلى الله عَنْ الله عَنْ الله عَنْ الله
٩٤٥٦٤٩. الصادرة بتاريخ 41.45.١٠٤٩. يدوه	الحامل (ة) لبطاقة التعريف الوطنية رقم: ٨٠٨.
قسم: علوم المادة:	المسجل بكلية: على ١٠٠٠ المد فيقتم

The aim of this wor his study the effect of Alemannium and living Coball-doping, as well as their consequences, on the properties of Fine Oxidethin It

أصرح بشرفي أني ألتزم بمراعاة المعايير العلمية والمنهجية ومعايير الأخلاقيات المهنية والنزاهة الأكاديمية المطلوبة في انجاز البحث المذكور أعلاه وفق ما ينص عليه القرار رقم 1082 المورخ في 2021/12/27 المعدد للقواعد المتعلقة بالوقاية من السرقة العلمية ومكافحتها.

التاريخ: 10 ... 60 ... 2202.

إمضاء المعني بالأمر